CHEMISTRY OF MATERIALS
Review

Chem. Mater. **2011,** *23,* 501–515 501
DOI:10.1021/cm102196t

Recent Advances in Conjugated Polyelectrolytes for Emerging Optoelectronic Applications†

Aidee Duarte,[‡,§] Kan-Yi Pu,[⊥,§] Bin Liu,*[,⊥] and Guillermo C. Bazan*[,‡,#]

[‡]*Department of Chemistry & Biochemistry, Center for Polymers and Organic Solids, and* [#]*Department of Materials, University of California, Santa Barbara, California 93106, United States, and* [⊥]*Department of Chemical and Biomolecular Engineering, National University of Singapore, Singapore 117576.*
[§]*Both authors contributed equally to this work.*

Received August 3, 2010. Revised Manuscript Received September 28, 2010

This review summarizes recent advances in the science and applications of conjugated polyelectrolytes (CPEs), with an emphasis on direct visual sensing, cellular imaging, and the fabrication of optoelectronic devices. CPEs backbones that incorporate donor−acceptor units are useful for direct visual sensing, whereas CPEs with hyperbranched structures, or biocompatible long side chains, are particularly useful for cellular imaging. With specially designed counterions, CPEs also demonstrate unique function in device fabrication and operation, for example, in dye-sensitized solar cells (DSSCs), bulk heterojunction (BHJ) solar cells, polymer light-emitting diodes (PLEDs), polymer light-emitting electrochemical cells (PLECs), and organic thin film transistors (OFET). Additionally, new strategies to modify and optimize CPE properties for specific applications are provided. The work summarized herein not only illustrates relationships between molecular structures and function, but also highlights how the structural versatility of CPEs makes them a unique category of multifunctional materials with the potential for fulfilling a variety of optical and electronic applications in solution, mixed media, and in the solid state.

1. Introduction

Conjugated polyelectrolytes (CPEs) are defined as polymers having backbones with π-delocalized electronic structures and pendant substituents with ionic functionalities.[1] The properties of these materials combine the well-known complexity of polyelectrolytes, for which physicochemical properties depend on variable long-range electrostatic interactions,[2] with the rigid and highly hydrophobic nature of conjugated polymers (CPs). Unlike the majority of neutral CPs, CPEs can be dissolved in highly polar solvents. This feature opens unique possibilities in emerging technologies. For example, certain CPEs are water soluble, and can therefore be introduced into homogeneous or heterogeneous assays that are responsive toward specific biomolecular targets.[3] The unique electronic characteristics of the backbone provide a combination of large optical cross section with facile interchain and intrachain excitation transfer.[4] It is therefore possible to create fluorescent assays with sensitivities above those obtained with widely used small molecular dyes and lower limits of detection.

Similarly, the use of polar solvents allows deposition of CPEs atop neutral organic semiconductors with orthogonal solubility.[5] Little disruption of underlying layers is achieved and it is therefore relatively simple to fabricate multilayer devices using solution deposition methods. These considerations have been particularly useful for the design and fabrication of polymer light-emitting diodes (PLEDs) that require an electron injection/transport layer and the use of stable high work function cathodes.[6] The presence of ions within the integral composition of CPEs is important for achieving electronic function that is not attainable with their neutral counterparts. For instance, ion motion can redistribute the electric fields within a device.[7] Alternatively, it is possible to obtain aligned dipole layers at organic/metal interfaces that effectively modify the work function of the electrode.[8] The degree to which each of these mechanisms is operative remains under debate, but it is likely to be dependent on the layer thickness, choice of counterion and the organization of the hydrophobic backbone.

The combination of scientific complexity and the opportunities to overcome bottleneck problems that limit widespread implementation of "plastic electronics" and to design new types of biosensor and biological imaging materials make CPEs meaningful subjects of contemporary polymer research. The publications and citations are increasing in number, and recent reviews have appeared that summarize relevant previous work.[9] The goal of this focused review is to highlight recent advances published in the last two years that are not covered in previous reviews. Special emphasis has been placed on the use of CPEs in sensing, cell imaging, and electronic devices with a focus on the mechanism of function, rather than a comparison of device performance. Because of space

† Accepted as part of the "Special Issue on π-Functional Materials".
*cheliub@nus.edu.sg, bazan@chem.ucsb.edu.

Published on Web 11/09/2010

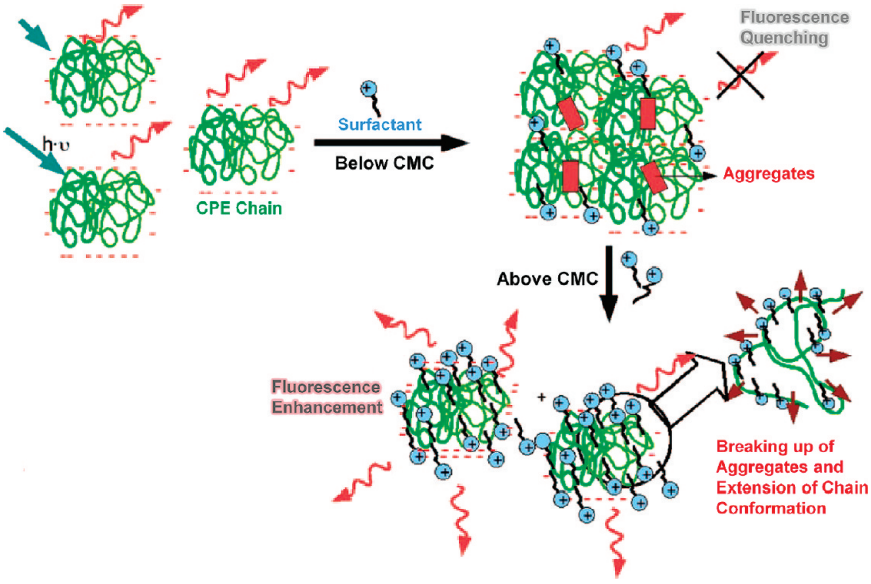

Figure 1. Proposed mode for the interactions between oppositely charged CPEs and surfactants at different concentrations. Reproduced with permission from ref 11. Copyright 2008 American Chemical Society.

limitations, it is not possible to describe all of the CPE publications and we apologize in advance for any omissions that may have occurred.

2. Strategies to Modify and Optimize CPE Properties

The addition of surfactants is a simple way to fine-tune the optical properties of CPEs. The resulting CPE/surfactant complexes can display different sizes, chemical compositions and conformations, depending on the concentration and nature of the participating species.[10] As illustrated in Figure 1, for oppositely charged CPE and surfactants, at low surfactant concentrations, strong static fluorescence quenching of the CPE has been observed as a result of charge pairing and concomitant formation of aggregates.[11] As the surfactant concentration is increased to above its critical micelle concentration (CMC), fluorescence enhancement is observed due to transformation of the initially formed polymer aggregates into new species within which polymer segments are possibly separated by the surfactant molecules.[12] On the other hand, addition of a nonionic surfactant, e.g., *n*-dodecylpentaoxyethylene glycol ether to CPE solutions can also increase the polymer fluorescence regardless of the surfactant concentration.[13,14] In addition, surfactants have also been employed to organize CPE chains in films. The complexation between an anionic derivative of poly(9,9-dioctylfluorene) (**A1**, Scheme 1) and 3-(*N*,*N*-dimethyloctylammonio)propanesulfonate inner salt[15] led to lamellar structural features, which were confirmed by using small-angle X-ray scattering measurements and atomic force microscopy (AFM). Based on these findings, surfactants have been utilized as additives to enhance fluorescence quenching[16]and energy transfer efficiencies,[17]which have applications in enzyme activity assays.[18]

A very recent strategy to increase the optical output from CPEs is the application of metal-enhanced fluorescence (MEF). MEF results from the interactions between fluorophores and surface plasmons in metallic nanostructures (e.g., Ag and Au), which amplify the incident electric field and accelerate radiative decay rates.[19] Substrate preparation begins with the immobilization of negatively charged Ag nanoparticles (NPs) onto NH_3^+-functionalized quartz slides (Figure 2).[20] A polyelectrolyte layer-by-layer process[21] using poly(diallyldimethyl ammonium chloride) (PDDA) and poly(sodium 4-styrenesulfonate) (PSS) was then used to modify the distance between the Ag NPs and a cationic poly(fluorene-*alt*-benzothiadiazole) (PFBT, **A2** in Scheme 1) layer. As compared to the photoluminescence (PL) intensity from **A2** adsorbed on a quartz slide, the initial build-up of the spacer from one to two bilayers (BLs) (~6−7 nm) led to a 3-fold increase in intensity, followed by a decrease upon further increase to three and four BLs. The NP amplified CPE emission was utilized to develop a sensing surface, which resulted in selective detection of single-stranded DNA (ssDNA) with a higher signal output, as compared to that obtained by using **A2** on a plain quartz surface.

Ion exchange constitutes a simple method to adjust the optical and electronic properties of CPEs. Introducing large anions with a cationic CPE leads to increases in the PL quantum yields and makes the optical features less sensitive to the environment, presumably due to a reduction in interchain contacts.[22] Further mechanistic insight into the influence of ions on fundamental photophysical processes was recently published by Friend and co-workers, who studied a CPE copolymer (**A3**, Scheme 1) derived from **A2**, in which only a limited number of repeat units contained the ionic functionalities.[23] A combination of time-resolved PL spectroscopy and transient absorption measurements suggests that emission quenching typically observed with CPEs can be explained by the formation of charge-transfer states that are stabilized by the Coulomb field of the ions. The nature of the charge compensation counterions was also found to be a useful molecular

Scheme 1. Chemical Structures of CPEs A1−A8

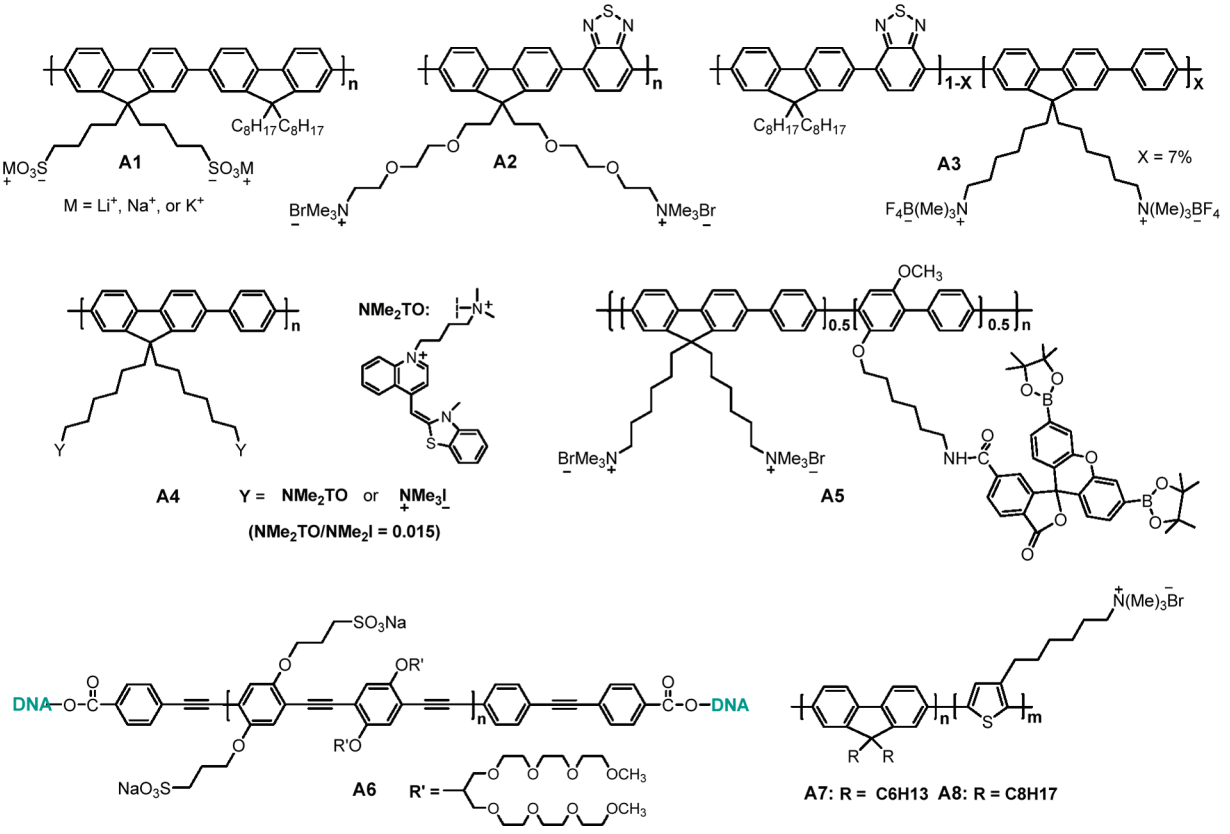

variable to modulate the structures of CPE/dye-labeled DNA complexes at the molecular scale,[24] the charge carrier mobilities in thin films, and the performance of PLEDs.[25]

Attaching fluorophores with biorecognition capabilities is an up and coming strategy to endow CPEs with improved sensing capabilities. A CPE bearing an intercalating dye (**A4**, Scheme 1) was recently reported to recognize double-stranded DNA (dsDNA) from ssDNA in serum-containing media.[26] This sensing ability stems from the substantial fluorescence enhancement of the dye (thiazole orange, TO) upon dsDNA intercalation and the subsequent in situ energy transfer from the conjugated backbone to TO. Wang's group also reported a CPE substituted with a boronate-protected fluorescein (**A5**, Scheme 1) for the detection of hydrogen peroxide and glucose in serum.[27] Both studies illustrate the remarkable potential for the development and design of new CPEs with chemically responsive modules that allow target detection in complex biological media.

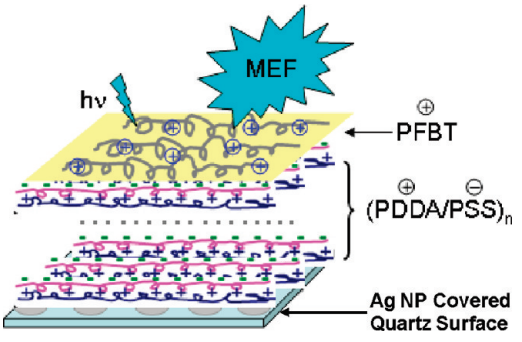

Figure 2. Schematic illustration of the CPE-Ag NP platform. In the original figure PFBT corresponds to **A2**. Reproduced with permission from ref 20. Copyright 2010 Wiley-VCH Verlag GmbH & Co. KGaA.

Kim's group attached single-stranded oligonucleotides to both ends of an anionic poly(p-phenyleneethynylene) (PPE) via carbodiimide-mediated coupling reaction (**A6**, Scheme 1).[28] Upon hybridization with a dye-labeled complementary DNA, efficient energy transfer from the PPE-DNA hybrid to the dye occurred, allowing efficient DNA detection. The same group also reported a peptide oligomer pentatyrosine functionalized PPE.[29] These efforts illustrate the feasibility of developing fluorescent conjugates using carboxyl end-capped CPEs, whereas their potential biological applications remain to be explored.

Block copolymers incorporated with CPE segments constitute yet another class of materials with unique structural handles to fine-tune relevant properties. Scherf's group synthesized a series of block copolymers comprising an organo-soluble polyfluorene (PF) block chemically bound to a cationic polythiophene (PT) segment (**A7** and **A8**, Scheme 1).[30] Both absorption and emission spectra of **A7** in tetrahydrofuran change upon addition of hexane or water, illustrating the formation of different supramolecular structures, that display different levels of energy transfer between the organo-soluble PF segment and the water-soluble PT. These block copolymers tend to self-assemble into layered aggregates in solution and in the solid state.[31]

3. Direct Visual Sensing

The majority of CPE-based assays take advantage of polymer fluorescence quenching via electron/energy transfer mechanisms,[3,32] or analyte-induced polymer aggregation as the transduction mechanism for target detection.[33] CPE-based assays involving Förster resonance energy transfer (FRET) have been extensively developed and reviewed.[9] Much of the FRET work was stimulated by the demonstration of specific DNA sequence detection using a dye-labeled peptide nucleic acid (PNA) probe and cationic poly(fluorene-*alt*-phenylene) (PFP).[34] On the other hand, by virtue of the sensitive conformation-dependent absorption properties of the PT backbone, Leclerc's[35] and Inganäs,[36] groups have developed colorimetric assays for DNA sensing. Colorimetric discrimination of other targets such as proteins,[37] peptide,[38] adenosine triphosphate (ATP),[39] amines,[40] folic acid,[41] and heparin,[42] has also been realized using water-soluble PT derivatives. Despite the availability of several types of CPE-based assays, fast, simple, and instrument-free direct visual sensing strategies remain of great interest and importance.

CPEs containing backbones with donor−acceptor architectures constitute a recent advance for direct visual detection. The molecular design is guided by the hypothesis that interchain FRET should be more efficient than intrachain FRET due to stronger electronic coupling and the increased dimensionality for interchain vs intrachain interactions. A cationic PFP derivative containing 5 mol % 2,1,3-benzothiadiazole (BT) units (**B1,** Scheme 2) was first synthesized for multicolor DNA detection[43] and DNA quantification.[44] In dilute solutions, the polymer emits blue fluorescence (Figure 3). Complexation between the CPE chains and oppositely charged DNA molecules induces polymer aggregation, leading to enhanced interchain contacts and improved electronic coupling between optical partners. Under these conditions, energy transfer from the fluorene segments (donor) to the BT units (acceptor) is more efficient than in isolated chains, and thus green emission dominates the solution fluorescence. Such an aggregation-enhanced FRET allows **B1** to effectively quantify dsDNA ranging from 0.6 nM to 0.15 μM in terms of base pairs.[44] To extend the quantification range of DNA, Bazan et al. synthesized a new BT-containing polymer (**B2**, Scheme 2) to have a higher charge density with oligo(ethylene oxide) pendant groups on the phenylene units.[45] This structural modification led to a significant improvement in water-solubility for **B2** as compared to that for **B1**. As a result, the calibration range was successfully extended to allow determination of dsDNA concentration from 0.003 nM to 20 μM.

By taking advantage of the electrostatic attraction between CPEs and biomolecule-induced aggregation, Liu's group synthesized a BT-containing CPE (**B3**, Scheme 2) for heparin quantification and discrimination from its structural analogue hyaluronic acid.[46] As shown in Figure 4a, with increasing heparin concentration, the orange emission band at 595 nm progressively grows at the expense of the blue emission band at 415 nm. Moreover, changes in the PL spectra can be monitored by simple visual inspection under a portable UV-lamp, as shown in Figure 4b. Utilization of **B4** (Scheme 2), with exclusively cationic oligo(ethylene oxide) side chains, further increased the upper detection limit from 48 μM (**B3**) to 76 μM.[47] In addition, a carboxyl BT-based CPE (**B6**) has also been designed to have different responses to proteins, and display emission from blue to yellow, green, or dark in the presence of lysozyme, bovine serum albumin (BSA), and cytochrome *c*, respectively.[48] Similarly, Swager's group synthesized an anthryl-doped carboxyl PPE (**B5**, Scheme 2), which exhibits blue-to-green fluorescence changes in the presence of multicationic amines (spermine, spermidine, and neomycin).[49]

BT-containing CPEs have been utilized as ratiometric probes to monitor enzyme activity. This concept was demonstrated by Wang's group by using the anionic ATP and alkaline phosphatase as the substrate and enzyme, respectively.[50] Addition of the substrate into the solution of **B1** induces a fluorescence color variation from blue to green (Figure 5). After substrate cleavage by the enzyme, the electrostatic attraction between the substrate fragments and the CPEs becomes weak, ultimately failing to induce compact polymer aggregation. As such, FRET from the fluorene units to the BT sites is reduced, leading to the recovery of blue fluorescence for the polymer solution (Figure 5). The same group also synthesized an anionic BT-containing CPE (**B7**, Scheme 2) for positive substrate-based enzyme activity studies.[51]

To gain insight into the aggregation-mediated fluorescence properties of BT-containing random CPEs, a carboxyl polymer (**B8**, Scheme 2) was synthesized whose net charge can be varied with the pH of solution.[52] Selective excitation of **B8** at the absorption maximum of BT units (440 nm) shows that the intrinsic BT emission in aqueous solution is enhanced with aggregation. This phenomenon illuminates that the BT emission is responsive to the polarity of the medium.

By virtue of environment-sensitive optical properties of BT emission, BT-based alternating CPEs were synthesized as light-up probes for biomolecular quantification.[53] The polymers, including **A2** and **B9**−**B11** (Scheme 2), constitute anther category of CPEs that are applicable for direct visual sensing. Theoretical efforts have shown that the highest occupied molecular orbital (HOMO) energy level for **B9** is nearly delocalized over the π-conjugated systems, while the lowest unoccupied molecular orbital (LUMO) energy level is predominantly localized on the BT units.[54] These results implicate that the excitation of **B9** is accompanied by charge transfer from the fluorene segments to the BT units. As the local hydrophobicity of BT is significantly increased within aggregates, as compared to that in a well-separated molecular state, BT emission exhibits aggregation-enhanced fluorescence in polar aqueous solution.

The light-up responses of BT-based alternating polymers toward biomolecules, such as DNA and BSA were also investigated.[54] Addition of DNA or BSA to both **B9** and **B11** solutions leads to significantly increased

Scheme 2. Chemical Structures of CPEs (B1−B11) for Direct Visual Detection

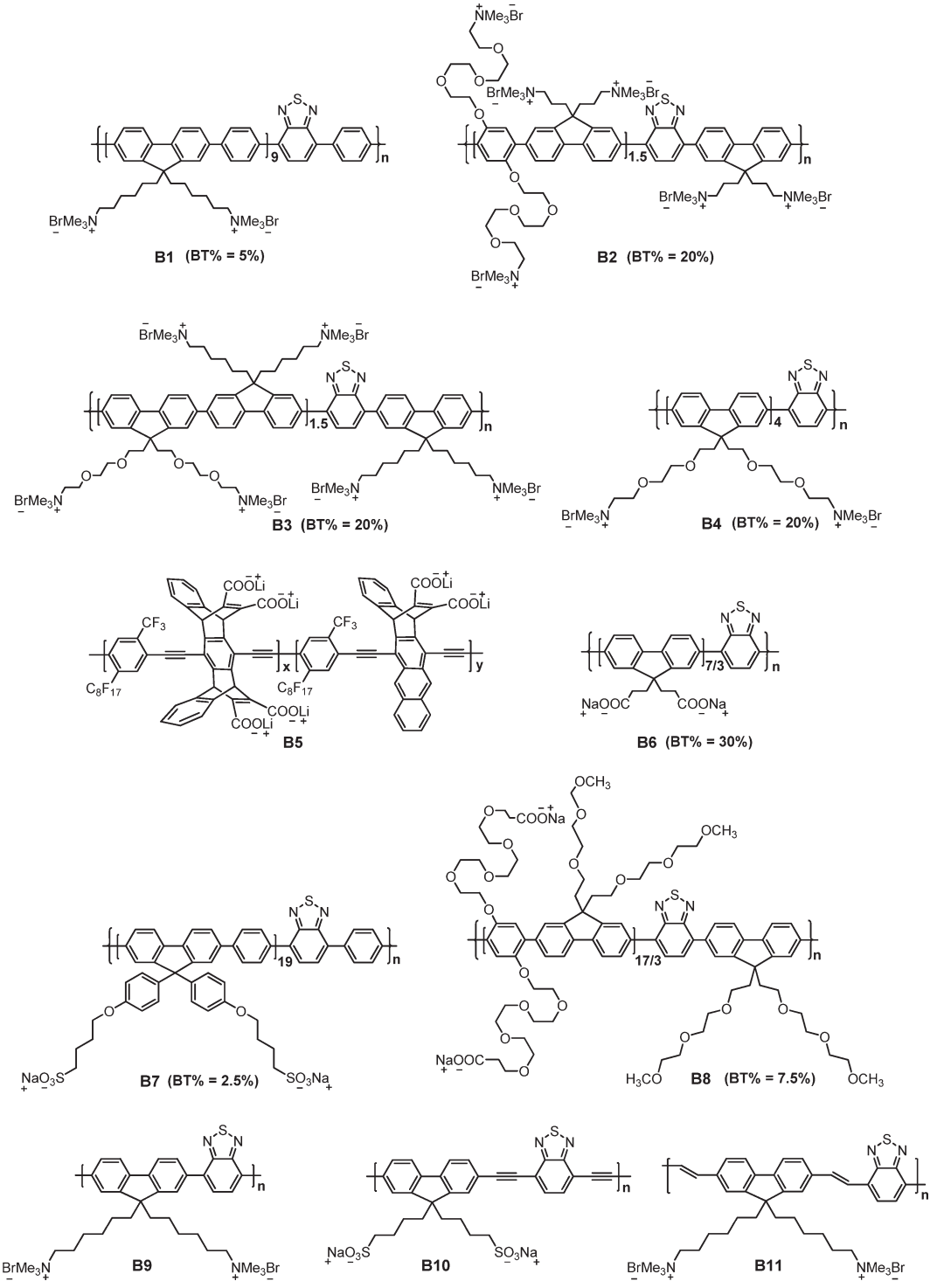

polymer fluorescence. The larger light-up responses of **B11**, as compared to that of **B9**, stems from the stronger charge-transfer character due to the presence of vinyl linkages along its backbone. These polymers exhibit multicolor light-up signatures toward different biomolecules as shown in Figure 6.[54] However, it is important to note that these CPEs are more appropriate for biomolecule quantification than for specific detection as the polymers do not contain specific recognition elements.[55]

4. Cell Imaging

The development of reliable fluorescent probes with high sensitivity and selectivity to decipher physiological processes and cellular structures is of central importance in scientific areas spanning from genomics to proteomics and pathophysiology. Because the existing fluorescence materials (e.g., small fluorophores, fluorescent proteins, and quantum dots) have their own disadvantages, such as low photobleaching thresholds, poor aqueous stability,

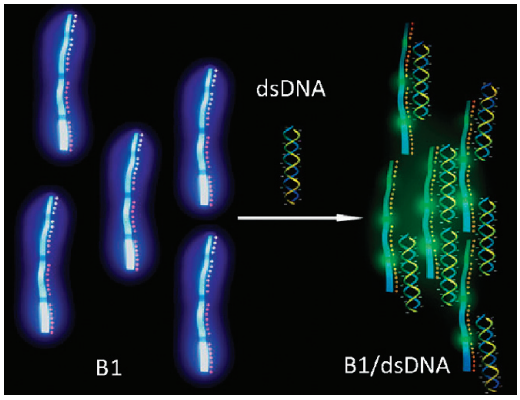

Figure 3. Illustration of the fluorescent color variation of **B1** upon addition of dsDNA. Reproduced with permission from ref 44. Copyright 2010 Wiley-VCH Verlag GmbH & Co. KGaA.

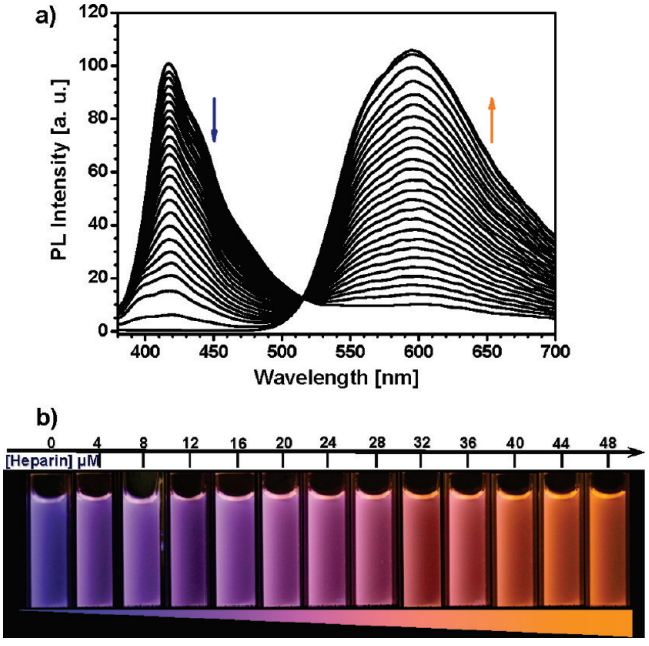

Figure 4. (a) PL spectra of **B3** at [RU] = 60 μM in 2 mM PBS at pH = 7.4 in the presence of [heparin] ranging from 0 to 50 μM at intervals of 2 μM (excitation at 365 nm); (b) Changes in the fluorescence of the corresponding solution at intervals of 4 μM under a hand-held UV-lamp with λ_{max} = 365 nm. Reproduced with permission from ref 46. Copyright 2010 American Chemical Society.

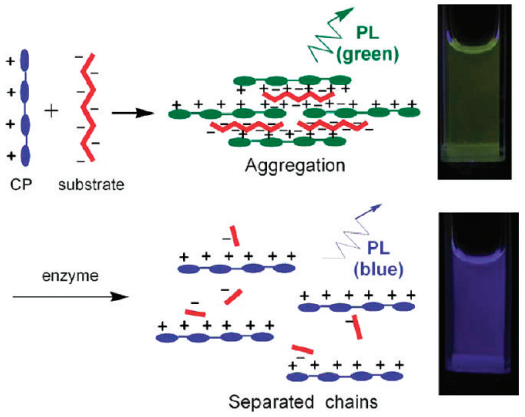

Figure 5. Illustration of the assay for enzymes and the cleavage of charged substrates based on BT-containing random CPE. Reproduced with permission from ref 50. Copyright 2007 The Royal Society of Chemistry.

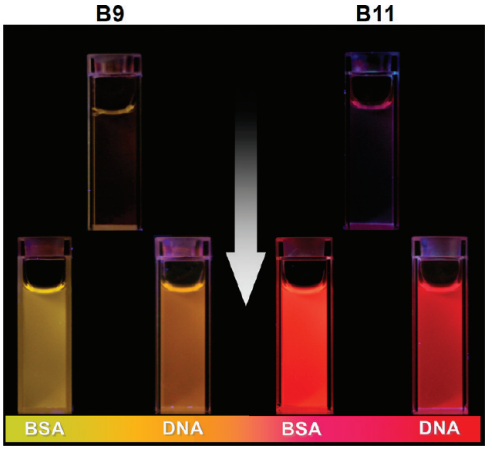

Figure 6. Photographs of emission from polymer solutions containing **B9** and **B11** ([RU] = 10 μM) in 2 mM PBS (pH 7.4) in the absence (up) and presence (bottom) of DNA or BSA (1.2 μM) under UV radiation at 365 nm. Reproduced with permission from ref 54. Copyright 2009 American Chemical Society.

and high cytotoxicity, new materials with improved properties remain in demand. In this regard, CPs have been reported to be promising cellular probes.[56] Recently, the application of CPEs in bioimaging has also been under intensive exploration. For instance, Nilsson and Inganäs et al. demonstrated that charged PTs are useful probes for specific staining of protein aggregates in tissue samples,[57] which is useful for monitoring protein-disordered pathogenic states, such as Alzheimer's disease and Parkinson's disease.

Targeted cellular imaging can also be realized by side-chain modification of traditional CPEs. Bunz's group reported an anionic folic acid (FA) substituted PPE (**C1**, Scheme 3) for in vitro imaging of cancer cells.[58] The performance of **C1** was compared with its counterpart (**C2**, Scheme 3) without FA groups. Confocal laser scanning microscopy (CLSM) experiments showed that **C1** served as an effective probe to selectively stain KB cancer cells through receptor mediated uptake (Figure 7). In contrast, **C2** exhibited nonspecific cellular internalization for both KB cancer cells and NIH-3T3 normal cells due to nonspecific interactions with the cellular surfaces. This study nicely demonstrated the potential of CPEs for bioimaging applications.

Traditional CPEs without biorecognition elements may also exhibit intracellular targeting capabilities. Bunz and Fahrni et al. found that **C3** (Scheme 3) could selectively stain the extracellular matrix protein fibronectin of live fibroblast cells by taking advantage of low-affinity polyvalent interactions between the carboxyl groups of **C3** and the positively charged extended area within fibronectin repeats 12−14, a location involved in binding of heparin.[59] Similarly, Björk and Nilsson et al. also observed specific intracellular targeting behaviors for anionic, cationic and zwitterionic PT derivatives (**C4**−**C6**, Scheme 3). For instance, both **C5** and **C6** directly

Scheme 3. Chemical Structures of CPEs (C1−C9) for Cellular Imaging

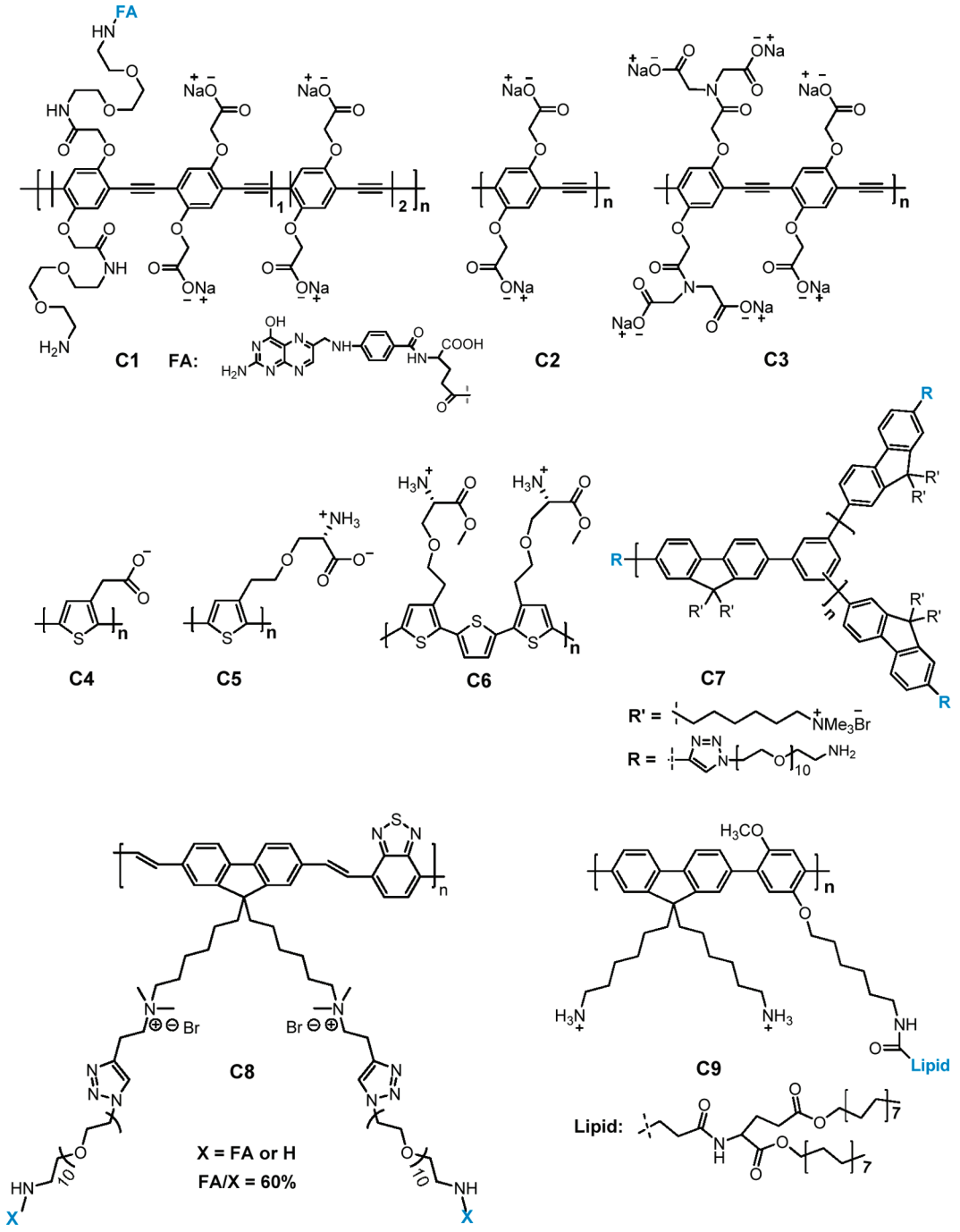

target cytoplasmatic vesicles in cultured fibroblasts and macrophages after fixation (Figure 8).[60] The fact that all the PT derivatives bind almost equally well regardless of their charged natures suggests that this targeting ability should arise from the PT backbone rather than from the side chains. Of particular interest is that **C4** can also stain the cytoplasmatic vesicles of living cells. However, the underlying mechanism and the detailed molecular state of the polymers in the cytoplasmatic vacuoles is elusive and requires further investigation.

CPEs with spherical molecular architectures or self-assembled nanostructures have also been designed to facilitate their application in cellular imaging. Liu's group reported a double-ingredient hyperbranched CPE (**C7**, Scheme 3) for this purpose.[61] With a fluorescent CPE core and poly(ethylene glycol) (PEG) shells, **C7** intrinsically forms single-molecular core−shell nanospheres with an average diameter of ~11 nm as determined by transmission electron microscopy (TEM) (Figure 9a). Using the breast cancer cell line MCF-7 as an example, **C7** can be internalized efficiently and accumulated in the cytoplasm to give bright fluorescence (Figure 9b). These single-molecular nanospheres also have good photostability, high quantum yields (30% in buffer), good biocompatibility, and low cytotoxicity. Subsequently, the same group synthesized a molecular brush that contains a

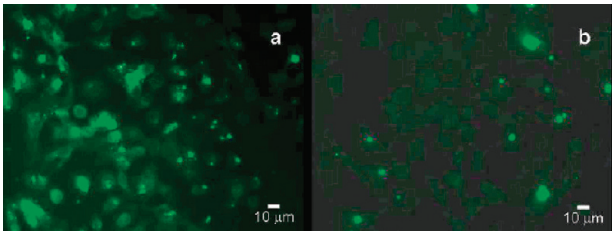

Figure 7. CLSM images of KB cells after incubation with (a) **C1** or (b) **C2**. Reproduced with permission from ref 58. Copyright 2007American Chemical Society.

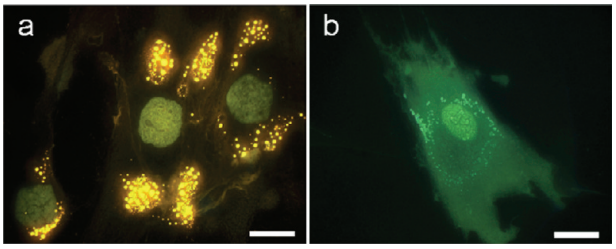

Figure 8. CLSM images of human fibroblasts stained with (a) **C6** after EtOH:HAc fixation; (b) **C5** after acid formalin alcohol fixation. Scale bar: 20 μm. Reproduced with permission from ref 60. Copyright 2007 Elsevier.

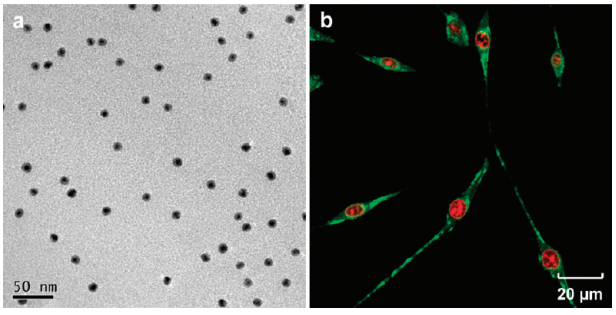

Figure 9. (a) TEM image and (b) CLSM image of MCF-7 cells costained by **C7** and propidium iodide (PI). Reproduced with permission from ref 61. Copyright 2009 American Chemical Society.

far-red/near-infrared (NIR) CPE backbone and PEG side brushes (**C8**, Scheme 3) with terminal folic acid groups.[62] This molecular brush has the emission maximum at 635 nm, and can self-assemble into nanoparticles with an average size of 130 nm in aqueous solution. It allowed for effective visualization and discrimination of MCF-7 cancer cells from NIH-3T3 normal cells in a high contrast, selective, and nonviral manner.

Wang's group extended the structural diversity by synthesizing a cationic CPE with lipid side chains (**C9**, Scheme 3) for cellular imaging.[63] Because of the amphiphilic nature of the lipid, **C9** self-assembles into nanoparticles with diameter of 50 nm in aqueous solution. **C9** has been applied as a vector to deliver genes into A549 cells and probe the expression of proteins. A plasmid containing cytomegalovirus enhancer and enhanced green fluorescent protein (pCX-EGFP) was used in these experiments. Electrostatic attraction between **C9** and pCX-EGFP leads to nanoparticle complexes with the plasmid molecules on the surface. After incubation of the **C9**/pCX-EGFP complex with the cells, the nanoparticle complex was internalized by the cells. Under the intracellular environment, the pCX-EGFP is gradually released from the surface of the nanoparticle, ultimately entering the cellular nucleus to perform transfection.

5. Device Application

5.1. Dye-Sensitized Solar Cells. In addition to various biological applications, CPEs are becoming new players in the development of optoelectronic devices. In this regard, CPEs have been used as effective light-harvesting sensitizer materials for dye-sensitized solar cells (DSSCs). DSSCs are low cost energy devices with high light-to-electrical conversion efficiencies, which were first reported by Grätzel et al in 1991.[64] Up to now, DSSCs with over 11% efficiency have been achieved with TiO_2 photoanode on glass substrate.[65] A typical DSSC comprises of a dye-sensitized semiconductor photoanode, an electrolyte containing redox couple and a counter electrode. The dye is one of the key components in DSSCs, which takes care of light absorption process and charge separation process in DSSCs. So far, the majority of research on organic dyes is focused on small molecules.[66] The reported CPE-based dye sensitizers generally have carboxylic acid on the side chains to anchor onto the porous nanocrystalline TiO_2 surface. Schanze and Reynolds's groups have conducted pioneering work in CPE-based DSSCs.[67,68] To study the structure−property relationship of CPEs in DSSCs, these groups systematically investigated the device performance of a series of carboxylated poly(arylene-ethynylene)s **D1**−**4** (Scheme 4). TiO_2/CPE films were tested in DSSCs using an I_3^-/I^- propylene carbonate electrolyte and a Pt/FTO counter electrode. The power conversion efficiencies (PCEs) under AM1.5 illumination (100 mW/cm^2) for **D1**−**4** were measured to be 0.34, 0.53, 0.58, and 0.33, respectively. The trend in PCE is generally consistent with the red-shift in polymer absorption, whereas the lower PCE for **D4**, as compared to that for other CPEs, was ascribed to exciton trapping in polymer aggregates.

Liu's group also reported CPE-based DSSCs using **D5** as the dye sensitizer.[69] **D5** contains 30% BT units and displays the maximum absorption at 444 nm, which gave 1.39% efficiency in liquid electrolyte based DSSCs. More recently, carboxylated **D6** was prepared with a donor-π-acceptor structure that was specifically designed for DSSC application.[70] **D6** has an electron donating backbone (triphenylamine) and an electron accepting side chain (cyanoacetic acid) with conjugated thiophene units as the linkers. Computational efforts revealed that the HOMO of **D6** is delocalized on the polymer backbone, whereas the LUMO is mainly localized on the acceptor side chain. This electron redistribution between the HOMO and LUMO leads to a pronounced intramolecular charge separation for this transition, which is beneficial for electron injection into the TiO_2 layer. The **D6**-based DSSC exhibits a PCE of 3.5%, which is the highest efficiency achieved so far for DSSCs using CPEs as the sensitizers.

Scheme 4. Chemical Structures of CPEs (D1-D15) for Device Applications

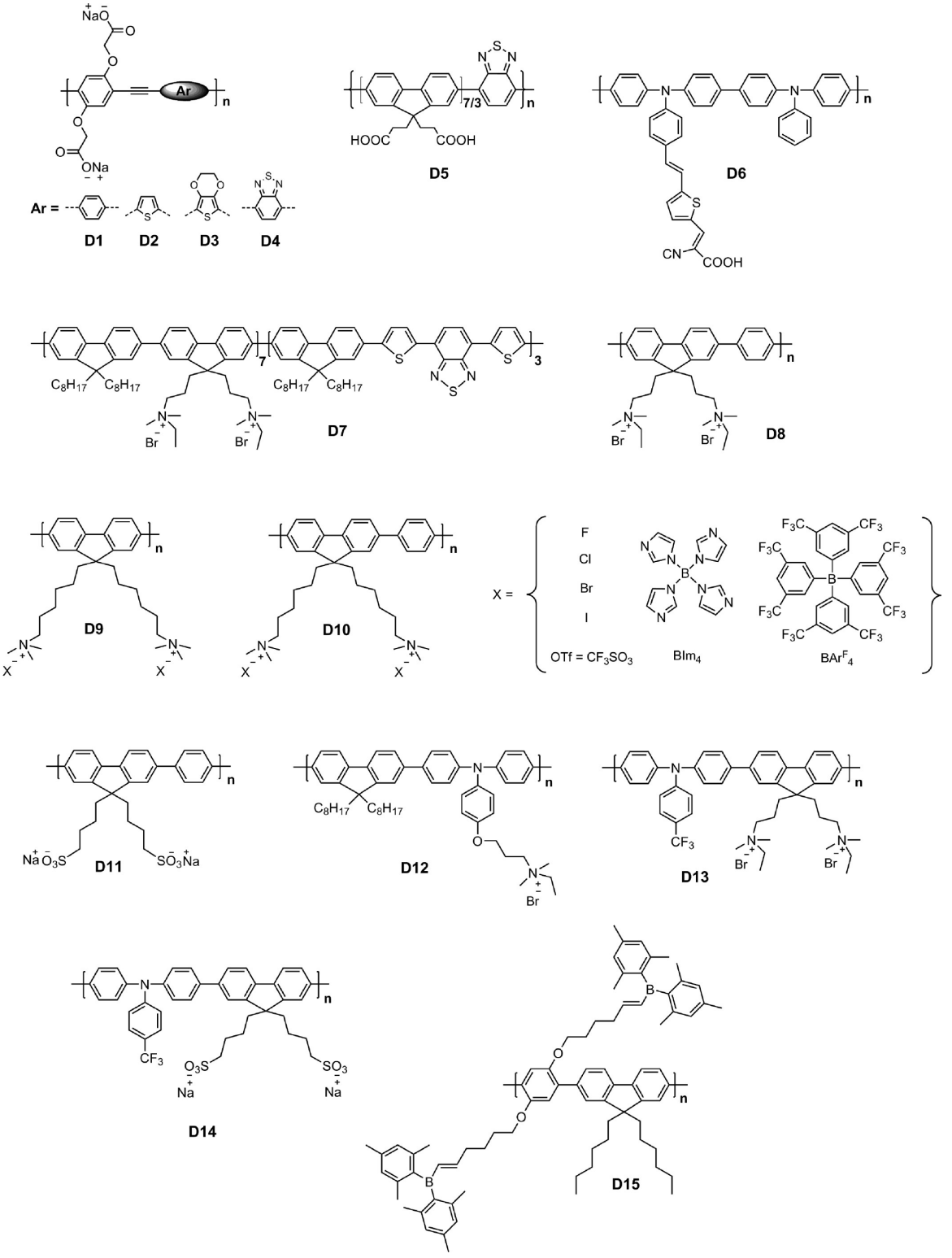

5.2. Bulk Heterojunction Solar Cells. Bulk heterojunction (BHJ) solar cells based on interpenetrating blends of electron- and hole-transporting materials are promising devices for low-cost and sustainable electricity production.[71] Central to this type of organic photovoltaic technology is the optimization of the short circuit current density (J_{SC}), open circuit voltage (V_{OC}), and fill factor (FF), which influence the PCE as shown in eq 1

$$\mathrm{PCE} = \frac{V_{OC} J_{SC} \mathrm{FF}}{P_{in}} \quad (1)$$

where P_{in} is the incident light power. Cao and co-workers demonstrated that the V_{OC} can be increased by up to 0.3 V

in solar cells by integrating a 5 nm CPE interlayer of **D7** or **D8**, shown in Scheme 4, relative to the situation in control devices.[72] Specifically, solar cells with poly[2,7-(9,9-dioctyl-fluorene)-*co*-(4,7-dithien-2-yl)-2,1,3-benzothiadiazole]/[6,6]-phenyl-C_{61}-butyric acid methyl ester (PFO−DBT-35/PCBM) as the active layer showed V_{OC} values of 0.95 and 1.00 V for **D7** and **D8** interlayers, respectively, leading to PCE values of 1.9% and 2.1%, respectively. For comparison, the control device yielded a V_{OC} of 0.65 V and a PCE of 1.0%. Fill factors and short-circuit current densities were also shown to increase slightly over the control device. Devices with the active layer poly[2,7-(9,9-dioctyl-fluorene)-*alt*-1,1-dimethyl-3,4-diphenyl-2,5-bis (2′-thienyl)-silole]/PCBM were also improved by introduction of the CPE layers, with PCEs of 2.6% and 2.5% for **D7** and **D8**, respectively. For comparison, the control device displayed a PCE of 1.7%. The superposition of the increased built-in potential across the device with the interfacial dipole from the CPE interlayer was believed to be responsible with the enhanced device characteristics.[72]

Insight into the origin of the increase in V_{OC} as a result of incorporating the CPE interlayer was sought by examining the dark currents of BHJ cells with different donor materials.[73] Thin films of **D9**, shown in Scheme 4, with various counterions were introduced into devices with general structure: indium tin oxide (ITO)/poly-(3,4-ethylenedioxythiophene)-poly(styrenesulfonate) (PEDOT:PSS)/active layer/CPE/Al. Different conjugated polymers: poly(3-hexylthiophene) (P3HT), poly[2-methoxy-5-(2′-ethyl-hexyloxy)-1,4-phenylenevinylene] (MEH-PPV), and PFO−DBT35,[70] were used as donor materials with PCBM as the acceptor. Devices with PFO−DBT35 showed V_{OC} of 1.07 V for **D9-Br** and **D9-OTf** and 1.06 V for **D9-BAr$^{F}_{4}$** and **D9-BIm$_4$**, an enhancement of 140 to 150 mV relative to control devices. These results are consistent with the studies described above. Cells with P3HT:PCBM or MEH-PPV:PCBM active layers with and without the CPE interlayer displayed equal V_{OC} values. These studies also showed that the increase in V_{OC} correlated to the dark $J-V$ characteristics. Devices with PFO−DBT35 displayed significantly suppressed dark current densities, 1−2 orders of magnitude, with the engineered CPE interlayer, whereas less than 1 order of magnitude was observed for P3HT:PCBM or MEH-PPV:PCBM. Although there is no exact model, as of now, that completely describes the effect of dark $J-V$ characteristics within the BHJ polymer solar cell, the authors suggest that the reduction of dark currents was responsible for the V_{OC} enhancement. Other polyfluorene polyelectrolyte derivatives were also incorporated as interlayers and were shown to behave similarly.[74] Despite mechanistic uncertainties, these findings point to a potentially important new application of CPEs in energy conversion technologies. Finally, it is worth mentioning that blends of cationic CPEs and PEDOT:PSS are currently being explored in inverted organic photovoltaic devices.[75]

5.3. Light-Emitting Diodes. The application of CPEs in PLEDs has been dominated by their use as electron injection/transport layers (ETLs) and studies toward understanding the mechanism by which charge injection

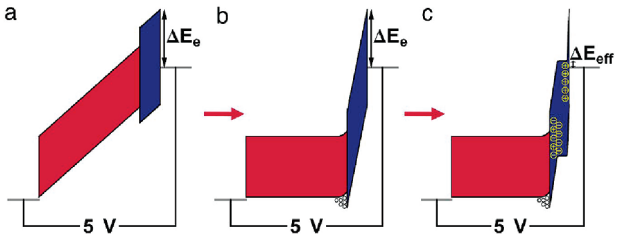

Figure 10. Response of an ITO/PEDOT/MEH-PPV/**D10-BIm$_4$**/Al device under 5 V applied bias; (a) Electric field (slope of the energy levels) is evenly distributed across the device; (b) Holes (open circles) accumulate at the MEH-PPV/**D10-BIm$_4$** interface, screening the electric field to the **D10-BIm$_4$** layer; (c) Ions (charges within the **D10-BIm$_4$** layer) then redistribute to screen the electric field to the two interfaces. Reproduced with permission from ref 76. Copyright 2008 The National Academy of Sciences of the USA.

barriers are decreased. A detailed set of experiments published by Hoven et al. revealed considerable subtleties on how ion motion and the energy levels of the internal PLED layers come together to improve device performance.[76] Briefly, these studies involved the use of an MEH-PPV emissive layer and various thickness of, **D10-BIm$_4$** (Scheme 4), as the ETL in ITO/PEDOT:PSS/MEH-PPV/**D10-BIm$_4$**/Au or Al devices. Examination of the temporal response and electric measurements of the devices led to the mechanism of action illustrated in Figure 10. The absence of a hole injection barrier at the ITO/PEDOT:PSS/MEH-PPV interface, Figure 10a, leads to facile injection. Accumulation of holes at the interface between MEH-PPV and the **D10-BIm$_4$**, shown in Scheme 10b, arises from the relative HOMO alignments. This accumulation of charge causes a screening of the internal electric field, essentially confining the potential drop within the CPE layer, as shown in Figure 10c. Also, redistribution of CPE counteranions leaves excess cations near the cathode that create a double charged layer in the CPE thin film. This ion motion causes a steep field gradient adjacent to the cathode, thereby facilitating electron injection. A faster temporal response observed with **D10-F** compared to **D10-BIm$_4$** is consistent with the rate of ion migration influencing the current densities. An interesting consequence of the mechanism is that hole and electron currents are diffusion currents rather than drift currents. It is important to note that the model assumes that the double layer is sufficiently thin to allow for efficient tunneling, and voltage drop across the ETL is equally distributed between the two interfacial double layers.

Electroabsorption spectroscopy was used to directly probe the electric fields within PLEDs containing **D10-F** as the ETL, i.e., ITO/PEDOT/MEH-PPV/**D10-F**/Al.[77] At voltages above the built-in voltage, one finds that the electric field in the emissive layer is screened. This is not the case for devices without the CPE ETL, for example ITO/PEDOT/MEH-PPV/Al or ITO/PEDOT/MEH-PPV/Ca/Al. These observations are consistent with screening of the external bias within the MEH-PPV because of hole accumulation and ion motion, entirely consistent with the model in Figure 10.

Studies on the hysteresis of V_{OC} measurements with **D9** as the ETL illustrate how the chemical nature of the

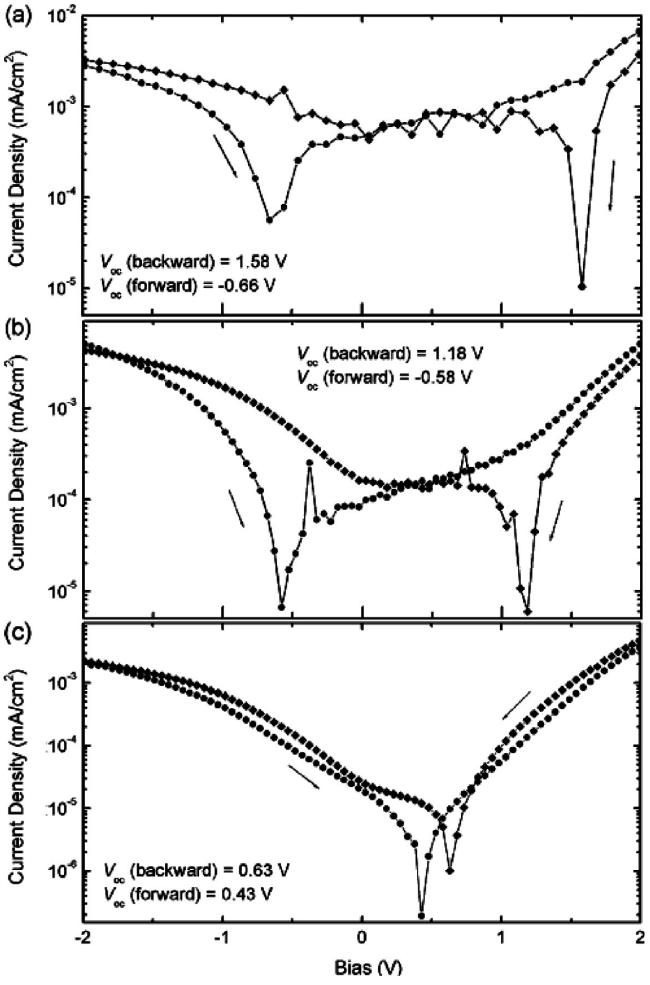

Figure 11. Current density under illumination as a function of bias plots obtained from devices with configuration ITO/PEDOT:PSS/MEH-PPV/**D9-BAr$^{F}_{4}$**/Al under scan rates of (a) 0.5 V/s, (b) 0.05 V/s, and (c) 0.01 V/s, measured right after holding the device at a forward bias of 3 V for 10 min. Reproduced with permission from ref 78. Copyright 2009 The Royal Society of Chemistry.

counterion influences the rate of ion migration and therefore PLED characteristics.[78] Specifically, Park et al. highlighted the influence of the scan rate on the measured V_{OC}. A larger hysteresis was observed with faster scan rates (Figure 11), consistent with a redistribution of ions. At slower scan speeds, ions have more time to respond, thus the experiment probes conditions are closer to equilibrium. In addition, the photocurrent hysteresis correlates with the size of the ion. A larger hysteresis was measured for **D9-BAr$^{F}_{4}$** than for **D9-OTf** or **D9-Br**.

An alternative mechanism for the improvement of electron injection by CPE ETL layers invokes a favorable, self-assembled, and permanent interfacial dipole at the CPE/metal interface. Such a dipole can cause a shift in the vacuum energy level, effectively reducing the electron injection barrier.[79] Studies probing the electronic properties and dipole formation at CPE/Au interfaces using ultraviolet photoelectron spectroscopy (UPS) were recently reported by Nguyen and co-workers.[80] They investigated a neutral CPE precursor, the quaternized cationic polymer derivatives, **D10-Br** and **D10-BIm$_4$**, and the anionic **D11,** depicted

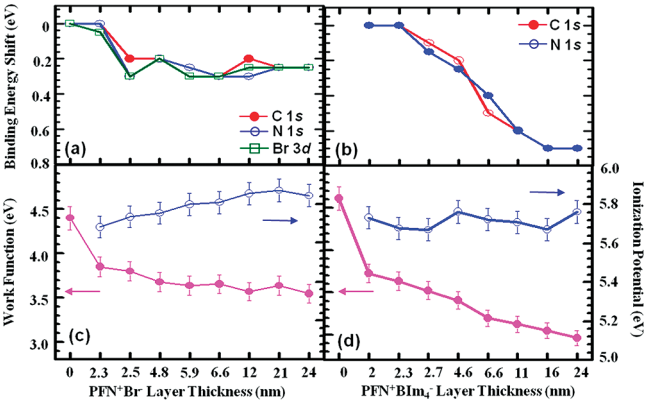

Figure 12. Binding energy shifts of XPS core levels versus (a) **D10-Br** and (b) **D10-BIm$_4$** layer thickness. Changes of the WF and IP in the (c) **D10-Br** and (d) **D10-BIm$_4$**. Reproduced with permission from ref 80b. In the original figure PFN^{+} corresponds to **D10**. Copyright 2009 Wiley-VCH Verlag GmbH & Co. KGaA.

in Scheme 4. A shift in the vacuum energy level (E_{vac}), extracted from the high binding energy cutoff of the UPS spectra, correlates to the presence of an interfacial dipole at the CPE/Au interface. Measurements revealed negligible dipoles for neutral **D10** and **D11**, whereas **D10-Br** and **D10-BIm$_4$** showed dipoles of −0.56 and −0.53 eV, respectively. In addition, examination of the UPS results shows differences in ionization potential (IP) and electron affinity relative in the thin films as a function of molecular structure, which were not observed with cyclic voltammetry. X-ray photoelectron spectroscopy (XPS) data, in conjunction with UPS measurements, yielded a detailed electronic picture at the CPE/Au interface as a function of film thickness. As shown in panels a and b in Figure 12, shifts in binding energy for 24 nm thick films of 0.25 and 0.70 eV toward higher binding energies were observed for **D10-Br** and **D10-BIm$_4$**, respectively. From vacuum level shifts and HOMO levels, the work function (WF) and the IP were plotted as a function of film thickness for **D10-Br** and **D10-BIm$_4$** shown in panels c and d in Figure 12, respectively. **D10-BIm$_4$**, had a smaller IP than **D10-Br** and a significant decrease in the WF of 1.43 eV compared to the decrease of 0.73 eV for **D10-Br**. This trend indicates a larger interfacial dipole and more pronounced band bending at the CPE/Au interface for **D10** with the larger counterions. The neutral precursor to **D10** and anionic **D11** had little WF and IP variation as a function of film thickness, indicating a lack of band bending.

Using near-edge X-ray absorption fine structure (NEXAFS) spectroscopy, the molecular orientation and composition at the topmost (2 nm) region of thin CPE films were probed.[81] A mild preferential "plane-on" orientation of the **D9** conjugated backbone, with respect to the surface, was observed for films atop MEH-PPV. More importantly, a larger accumulation of ionic component was observed for films atop the neutral MEH-PPV, as compared to ITO. It was surmised that the CPE backbone interacts more favorably with the hydrophobic MEH-PPV surface and that the charged counterions are

repelled to the topmost portion of the film. Assuming that these structural arrangements stay intact after the cathode deposition, the observed details are relevant for understanding the existence of a spontaneously formed aligned dipole layer that aids in charge injection.

Previous examination via AFM, focused ion beam TEM, and dynamic secondary ion mass spectroscopy revealed that the deposition of CPEs atop neutral conjugated polymers yield sharp interfaces, i.e there is little mixing of the two layers because of the solubility in solvents of very different polarities .[82] Additional insight was obtained by examination of CPE/MEH-PPV bilayers using resonant soft X-ray reflectivity, as reported by Wang et al.[83] As-cast interfacial bilayers of **D10-Br** and **D10-BIm$_4$** spun from methanol atop of MEH-PPV had smooth interfaces with average rms widths of 0.80 and 0.82 nm, respectively. These rms values were only slightly larger than the MEH-PPV reference layer. The chemical interdiffusion due to casting is limited to less than 0.6 nm, thereby creating interfaces nearly "molecularly" sharp, a remarkable achievement given that the layers are produced via solution deposition.

A series of structural modifications involving the conjugated backbone, charged pendant groups, and counterions has been examined in efforts to optimize the integration of CPEs in PLEDs. Cao and co-workers introduced a triphenyl-amine segment into the conjugated backbone, **D12**, modified the polymer's cationic charge density, **D13**, and even synthesized the anionic derivative **D14**, see Scheme 4 for polymer structures.[84] The triphenylamine groups were incorporated to improve the balance of electron and hole injection. Superior performance was observed for these modified polymers as the emitting layer in double-layer ITO/PEDOT:PSS (or polyvinylcarbazole)/CPE/Al (or Ba/Al) LED device configuration. Good quantum efficiency and luminescence was obtained from **D12** and **D13**, indicating balanced hole and electron transfer. **D12** with equal number of charges per triphenylamine was nearly independent to the type of anode buffer and cathode used, whereas **D13** with two charges per triphenylamine was dependent on the anode buffer. The increased electron injection observed for **D13** was attributed to the larger number of charged ammonium groups.

The anionic CPE modified with triphenylamine, **D14**, showed good hole-transport and electron-blocking capabilities. The relatively high HOMO (−5.22 eV) and LUMO (−2.26 eV) levels allow **D14** to be a good hole transporting layer, as well as a good electron-blocking layer. Better device performance was observed for **D14,** compared to PEDOT:PSS, in red and green emitting devices because of its higher LUMO level, which presumable makes it a better electron-blocking layer. The importance of energy level alignment was stressed, as devices that used blue emissive layer with HOMO and LUMO levels similar to **D14** showed similar device performance as those with PEDOT:PSS.

A study on the effect of halide counterions on PLED efficiencies using **D10** was undertaken by Garcia et al.[85] As the size of the counterion decreased (**D10-I** > **D10-Br** > **D10-Cl** > **D10-F**), PLED luminance and luminous efficiencies increased, while turn-on voltages decreased. To elucidate whether the effect was due to electron mobility, electrochemical stability of the counterions, or ion mobility, the charge transport characteristics were examined using single charge carrier diode configurations under a pulsed bias. No correlation between electron mobility and device performance was found. PLED performance with (steady bias) and without (pulsed bias) ion motion showed a reduction of efficiency with heavier halides. Interestingly, for **D10-I** and **D10-Br**, the device performance progressively decreased under continuous bias with increased current density. Counterion migration to the MEH-PPV/CPE interface, where there is hole accumulation, and the relative ease of oxidation for the different halide species is believed to be responsible for the deterioration in performance.

5.4. Organic Thin Film Transistors. Concepts learned from studies of PLEDs have led to CPE applications in organic thin film transistors[86] (OTFTs). The primary goal of this effort is to address limitations where contact resistances at the metal/organic semiconductor interfaces limit the performance of the devices.[87] This problem is particularly an issue under situations where high work function metals are incorporated into n-type devices. Device fabrication involves spin-casting **D10-X** (where X = F, Br, BIm$_4$) from methanol solutions atop PCBM followed by the deposition of Au source and drain electrodes, leading to the device depicted in Figure 13a. Examination of the transfer characteristics in Figure 13b demonstrates that despite the nearly absent change in total film thickness when deposited from a dilute solution, the presence of CPE leads to OTFTs with higher drain currents (I_{DS}), relative to untreated PCBM, and that there is little influence from the counteranions. From panels c and d in Figure 13, which show the output characteristics as a function of CPE thickness, one observes that proper gating behavior occurs only with thin CPE interlayers. Studies of the total resistance as a function of channel length revealed a substantial reduction of the contact resistance, from 13.5 MΩ for PCBM to 0.42 MΩ for **D10-F/PCBM**.[84] The reduction in contact resistance is attributed to the dipole formed from the thin CPE film which causes a downward shift of the vacuum level reducing the electron injection barrier. Care needs to be taken so that the CPE film does not interfere with the desired transistor gating behavior. Such a situation is observed with thicker films, where ion motion can redistribute electric fields and interfere with charge carrier transport.

5.5. Fixed p−n Junctions. New approaches for the design and construction of fixed organic p−n junctions are taking advantage of the unique semiconducting and ionic components of the CPE structure. Such junctions are fundamental modules in many of today's semiconductor devices, lead to diode characteristics and are attained when p-doped and n-doped materials come into contact with each other. Achieving bilayer p−n junctions with semiconducting polymers has been challenged by

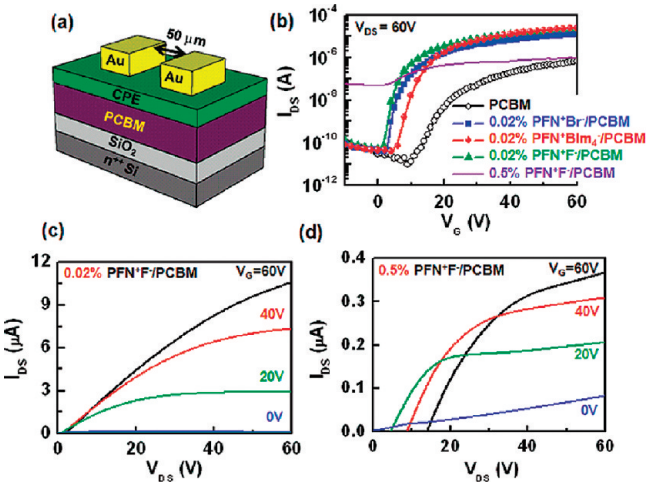

Figure 13. (a) OTFT test device that incorporates the CPE layer in between the source and drain electrodes and the n-type semiconductor PCBM. (b) Transfer characteristics at V_{DS} = 60 V as a function of counterions and concentration (for only **D10-F**). V_{DS} is the drain voltage, V_G is the gate bias, and I_{DS} corresponds to the source−drain current. (c, d) Output characteristics with **D10-F** layers deposited from 0.02% and 0.5% methanol solutions, respectively. The source−drain current, I_{DS} is plotted versus V_{DS} under different V_G. In the original figure PFN^+ corresponds to **D10**. Reproduced with permission from ref 86. Copyright 2009 American Chemical Society.

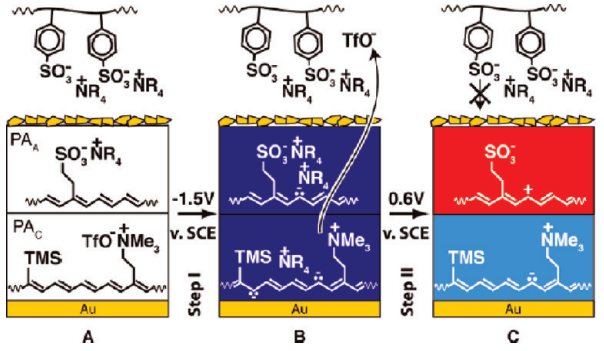

Figure 14. PMEC fabrication of a polyacetylene-based p−n junction using a tetrabutylammonium poly(styrene sulfonate) acetonitrile supporting electrolyte; (A) Initial undoped bilayer of solid films of a polyacetylene anionomer (PA_A) and a polyacetylene cationomer (PA_C) sandwiched between gold electrodes (top electrode in contact with PA_A is sufficiently thin so as to remain porous); (B) Structure following the application of −1.5 V vs SCE to the top porous electrode to n-doped the films; (C) Structure following the application of 0.6 V vs SCE to the top porous electrode to p-dope the PA_A layer in an internally compensated n-type form; complete reoxidation and p-doping of the PA_C layer is not possible because the original triflate (OTf-) anions were proviously lost to the solution and poly(styrene sulfonic acid) (PSS-) is too large to permeate the polymer film. Reproduced with permission from ref 89. Copyright 2010 American Chemical Society.

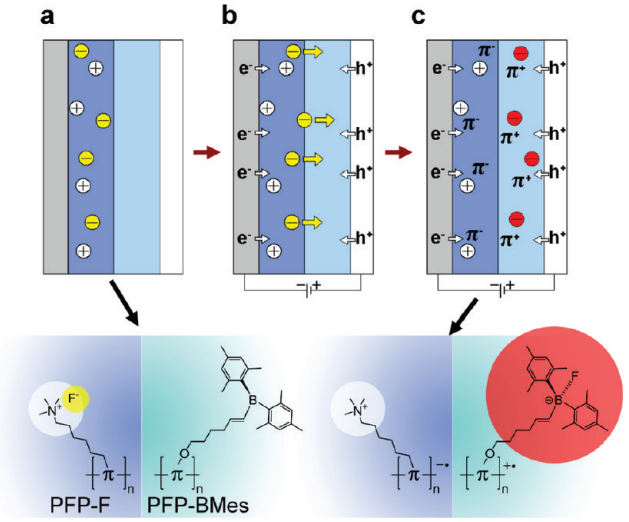

Figure 15. Schematic of the p-n junction formation: (a) Before an applied bias the device is as-cast; all ions are in the **D10-F** layer (dark blue layer), and the **D15** layer is neutral (light blue layer); (b) Under a positive applied bias electric field, the mobile fluoride anions (yellow) migrate into **D15**, while electrons are injected from the cathode (grey layer) and holes are injected from the anode (white layer); (c) Ions are compensated by injected charges creating p−n junction; a new immobile borate species (red) is formed, while the immobile quaternary ammonium cations (white) remain in place. In the original figure PFP-F and PFP-BMes correspond to **D10-F** and **D15**, respectively. Reproduced with permission from ref 90. Copyright 2010 Nature Publishing Group.

difficulties in the deposition of thin films with independent p-doped and n-doped layers.[88]

Creation of p−n junctions has been demonstrated by sandwiching mixed ionic−electronic conductors between gold electrodes, applying a bias and washing out the ions. By this method, the fabrication of the p-doped and n-doped layers are commensurate. A new method, polyelectrolyte mediated electrochemistry (PMEC), by which the n-doped and p-doped regions are generated independently, was reported by Lonergan and co-workers.[89] The PMEC method allows integration of different structures and extent of n-doping and p-doping. The formation of the p−n junction, detailed in Figure 14a−c, forms an internally compensated state, where the doped conjugated backbone is balanced by the charges on the pendant groups. The p−n junction exhibited diode behavior displaying no current with negative bias and high current for a positive bias, with ideality factors in the 3−3.5 range. A small photovoltaic effect was also measured. Rectification ratios (forward to reverse current at a particular voltage) as high as 900 were observed between 1 and 1.3 V.

Recently, CPEs have also shown to be a key ingredient in forming "fixed" p−n junctions by virtue of covalent chemical bond formation.[90] Bazan and co-workers designed a system where alcohol/water-soluble **D10-F** can be deposited atop a newly synthesized, organic soluble, poly(fluorene) with dimesitylboron functionalities attached to the side chains, **D15** shown in Scheme 4, as shown in Figure 15a. Upon application of an applied bias, the mobile fluoride ions move toward the **D15** layer, Figure 15b, wherein they form chemical bonds to the boryl pendant groups, Figure 15c. This bond permanently immobilizes the fluoride ions, producing a p−n junction consisting of a p-doped layer with borate counterions adjacent to an n-doped layer. The mechanism, corroborated by the initial turn-on time of 30 s and nearly instantaneous subsequent turn-on times, illustrates the initial time required for the ions to move and the subsequent permanent ion capture by covalent bonding. Thinner layers reach maximum luminance faster because the distance the fluoride ions must traverse is shorter.

6. Conclusion

The body of work reviewed here reveals that the unique structural attributes of CPEs can be utilized in a variety of emerging technologies. Many of these functions cannot be accomplished by using neutral conjugated polymer counterparts. There is much yet to be attained, both in terms of fully exploiting possible structural variations that embody recognition elements for new biological sensory and imaging applications, and in the elaboration of new optoelectronic device structures. Recent work has also taught us much about the electronic and optical properties in the solid state. This new basic science information promises to be a foundation for new applications, particularly in energy conversion technologies and energy efficient light-emitting devices. It will be well worth following closely future advances within this unique class of light-harvesting and semiconducting materials.

Acknowledgment. A.D. thanks The National Academies for their financial support through the Ford Foundation Diversity Fellowship. B.L. is grateful to the National University of Singapore (R-279-000-234-101, R279-000-301-646), Singapore Ministry of Education (R-279-000-255-112), and Ministry of Defense (R-279-000-301-232) for financial support. G.C.B. acknowledges generous support from the National Science Foundation (DMR 0606414).

References

(1) Pinto, M. R.; Schanze, K. S. *Synthesis* **2002**, *9*, 1293–1309.
(2) Barrat, J. L.; Joanny, J. F. *Adv. Chem. Phys.* **1996**, *94*, 1–66.
(3) (a) Gaylord, B. S.; Heeger, A. J.; Bazan, G. C. *Proc. Natl. Acad. Sci. U.S.A.* **2002**, *99*, 10954–10957. (b) Nilsson, K. P. R.; Rydberg, J.; Baltzer, L.; Inganäs, O. *Proc. Natl. Acad. Sci. U.S.A.* **2003**, *100*, 10170–10174. (c) Pinto, M. R.; Schanze, K. S. *Proc. Natl. Acad. Sci. U.S.A.* **2004**, *101*, 7505–7510. (d) Ho, H. A.; Doré, K.; Boissinot, M.; Bergeron, M. G.; Tanguay, R. M.; Boudreau, D.; Leclerc, M. *J. Am. Chem. Soc.* **2005**, *127*, 12673–12676.
(4) Swager, T. M. *Acc. Chem. Res.* **1998**, *31*, 201–207.
(5) Ma, W. L.; Iyer, P. K.; Gong, X.; Liu, B.; Moses, D.; Bazan, G. C.; Heeger, A. J. *Adv. Mater.* **2005**, *17*, 274–277.
(6) (a) Hoven, C.; Yang, R.; Garcia, A.; Heeger, A. J.; Nguyen, T. Q.; Bazan, G. C. *J. Am. Chem. Soc.* **2007**, *129*, 10976–10977. (b) Hou, L. T.; Huang, F.; Peng, J. B.; Wu, H. B.; Wen, S. S.; Mo, Y. Q.; Cao, Y. *Thin Solid Films* **2006**, *515*, 2632–2634.
(7) (a) Pei, Q. B.; Yu, G.; Zhang, C.; Yang, Y.; Heeger, A. J. *Science* **1995**, *269*, 1086–1088. (b) Smith, D. L. *J. Appl. Phys.* **1997**, *81*, 2869–2880. (c) Slinker, J. D.; DeFranco, J. A.; Jaquith, M. J.; Silveira, W. R.; Zhong, Y. W.; Moran-Mirabal, J. M.; Craighead, H. G.; Abruna, H. D.; Marohn, J. A.; Malliaras, G. G. *Nat. Mater.* **2007**, *6*, 894–899.
(8) Ishii, H.; Sugiyama, K.; Ito, E.; Seki, K. *Adv. Mater.* **1999**, *11*, 605–625.
(9) (a) McQuade, D. T.; Pullen, A. E.; Swager, T, M. *Chem. Rev.* **2000**, *100*, 2537–2574. (b) Liu, B.; Bazan, G. C. *Chem. Mater.* **2004**, *16*, 4467–4476. (c) Thomas, S. W., III; Joly, G. D.; Swager, T. M. *Chem. Rev.* **2007**, *107*, 1339–1386. (d) Bazan, G. C. *J. Org. Chem.* **2007**, *72*, 8615–8635. (e) Ambade, A. V.; Sandanaraj, B. S.; Klaikherd, A.; Thayumanavan, S. *Polym. Int.* **2007**, *56*, 474–481. (f) Herland, A.; Inganäs, O. *Macromol. Rapid Commun.* **2007**, *28*, 1703–1713. (g) Feng, F. D.; He, F.; An, L. L.; Wang, S.; Li, Y. L.; Zhu, D. B. *Adv. Mater.* **2008**, *20*, 2959–2964. (h) Nilsson, K. P. R.; Hammarström, P. *Adv. Mater.* **2008**, *20*, 2639–2645. (i) Ho, H. A.; Najari, A.; Leclerc, M. *Acc. Chem. Res.* **2008**, *41*, 168–178. (j) Hoven, C. V.; Garcia, A.; Bazan, G. C.; Nguyen, T. Q. *Adv. Mater.* **2008**, *20*, 3793–3810. (k) Pu, K. Y.; Liu, B. *Biosens. Bioelectron.* **2009**, *24*, 1067–1073. (l) Bunz, U. H. F. *Macromol. Rapid Commun.* **2009**, *30*, 772–805. (m) Jiang, H.; Taranekar, P.; Reynolds, J. R.; Schanze, K. *Angew. Chem., Int. Ed.* **2009**, *48*, 4300–4316. (n) Liu, Y.; Ogawa, K.; Schanze, K. S. *J. Photochem. Photobiol., C* **2009**, *10*, 173–190. (o) Li, K.; Liu, B. *Polym. Chem.* **2010**, *1*, 252–259. (p) Feng, X. L.; Liu, L. B.; Wang, S.; Zhu, D. B. *Chem. Soc. Rev.* **2010**, *39*, 2411–2419. (q) Huang, F.; Wu, H. B.; Cao, Y. *Chem. Soc. Rev.* **2010**, *39*, 2500–2521. (r) Duan, X. R.; Liu, L. B.; Feng, F. D.; Wang, S. *Acc. Chem. Res.* **2010**, *43*, 260–270. (s) Bunz, U. H. F.; Rotello, V. M. *Angew. Chem., Int. Ed.* **2010**, *49*, 3268–3279.
(10) (a) Treger, J. S.; Ma, V. Y.; Gao, Y.; Wang, C. C.; Wang, H. L.; Johal, M. S. *J. Phys. Chem. B* **2008**, *112*, 760–763. (b) Wu, M. Y.; Kaur, P.; Yue, H. J.; Clemmens, A. M.; Waldeck, D. H.; Xue, C. H.; Liu, H. Y. *J. Phys. Chem. B* **2008**, *112*, 3300–3310. (c) Dou, W. C.; Wang, C.; Wang, G. N.; Ma, Q.; Su, X. G. *J. Phys. Chem. B* **2008**, *112*, 12681–12685. (d) Zhang, T.; Fan, H. L.; Zhou, J. G.; Jin, Q. H. *J. Polym. Sci., Part A: Polym.* **2009**, *47*, 3056–3065.
(11) Laurenti, M.; Rubio-Retama, J.; Garcia-Blanco, F.; López-Cabarcos, E. *Langmuir* **2008**, *24*, 13321–13327.
(12) (a) Burrows, H. D.; Tapia, M. J.; Silva, C. L.; Pais, A. A. C. C.; Fonseca, S, M.; Pina, J.; Seixas de Melo, J.; Wang, Y.; Marques, E. F.; Knaapila, M.; Monkman, A. P.; Garamus, V. M.; Pradhan, S.; Scherf, U. *J. Phys. Chem. B* **2007**, *111*, 4401–4410. (b) Burrows, H. D.; Tapia, M. J.; Fonseca, S. M.; Pradhan, S.; Scherf, U.; Silva, C. L.; Pais, A. A. C. C.; Valente, A. J. M.; Schillen, K.; Alfredsson, V.; Carnerup, A. M.; Tomsic, M.; Jamnik, A. *Langmuir* **2009**, *25*, 5545–5556. (c) Ngo, A. T.; Cosa, G. *Langmuir* **2010**, *26*, 6746–6754.
(13) (a) Chen, L. H.; Xu, S.; McBranch, D.; Whitten, D. G. *J. Am. Chem. Soc.* **2000**, *122*, 9302–9303. (b) Burrows, H. D.; Lobo, V. M. M.; Pina, J.; Ramos, M. L.; Seixas de Melo, J.; Valente, A. J. M.; Tapia, M. J.; Pradhan, S.; Scherf, U. *Macromolecules* **2004**, *37*, 7425–7427.
(14) Al Attar, H. A.; Monkman, A. P. *J. Phys. Chem. B* **2007**, *111*, 12418–12426.
(15) Pace, G.; Tu, G. L.; Fratini, E.; Massip, S.; Huck, W. T. S.; Baglioni, P.; Friend, R. H. *Adv. Mater.* **2010**, *22*, 2073–2077.
(16) (a) Dalvi-Malhotra, J.; Chen, L. H. *J. Phys. Chem. B* **2005**, *109*, 3873–3878. (b) George, W. N.; Giles, M.; McCulloch, I.; de Mello, J. C.; Steinke, J. H. G. *Soft Matter* **2007**, *3*, 1381–1387.
(17) (a) Stork, M.; Gayloard, B. S.; Heeger, A. J.; Bazan, G. C. *Adv. Mater.* **2002**, *14*, 361–366. (b) Pu, K. Y.; Pan, Y. H. S.; Liu, B. *J. Phys. Chem. B* **2008**, *112*, 9295–9300. (c) Al Attar, H. A.; Monkman, A. P. *Adv. Funct. Mater.* **2008**, *18*, 2498–2509. (d) Pu, K. Y.; Zhan, R.; Liu, B. *Macromol. Symp.* **2009**, *279*, 48–51. (e) Nayak, R. R.; Nag, O. K.; Kang, M.; Jin, Y.; Suh, H.; Lee, K.; Woo, H. Y. *Macromol. Rapid Commun.* **2009**, *30*, 633–638. (f) Al Attar, H. A.; Monkman, A. P. *Biomacromolecules* **2009**, *10*, 1077–1083.
(18) (a) Liu, Y.; Schanze, K. S. *Anal. Chem.* **2008**, *80*, 8605–8612. (b) Liu, Y.; Schanze, K. S. *Anal. Chem.* **2009**, *81*, 231–239.
(19) (a) Stewart, M. E.; Anderton, C. R.; Thompson, L. B.; Maria, J.; Gray, S. K.; Rogers, J. A.; Nuzzo, R. G. *Chem. Rev.* **2008**, *108*, 494–521. (b) Aslan, K.; Gryczynski, I.; Malicka, J.; Matveeva, E.; Lakowicz, J. R.; Geddes, C. D. *Curr. Opin. Biotechnol.* **2005**, *16*, 55–62. (c) Lakowicz, J. R. *Plasmonics* **2006**, *1*, 5–33.
(20) Wang, Y. S.; Liu, B.; Mikhailovsky, A.; Bazan, G. C. *Adv. Mater.* **2010**, *22*, 656–659.
(21) Hammond, P. T. *Adv. Mater.* **2004**, *16*, 1271–1293.
(22) Yang, R. Q.; Garcia, A.; Korystov, D.; Mikhailovsky, A.; Bazan, G. C.; Nguyen, T. Q. *J. Am. Chem. Soc.* **2006**, *128*, 16532–16539.
(23) Hodgkiss, J. M.; Tu, G. L.; Albert-Seifried, S.; Huck, W. T. S.; Friend, R. H. *J. Am. Chem. Soc.* **2009**, *131*, 8913–8921.
(24) Kang, M.; Nag, O. K.; Nayak, R. R.; Hwang, S.; Suh, H.; Woo, H. Y. *Macromolecules* **2009**, *42*, 2708–2714.
(25) (a) Yang, R. Q.; Wu, H. B.; Cao, Y.; Bazan, G. C. *J. Am. Chem. Soc.* **2006**, *128*, 14422–14423. (b) Garcia, A.; T. Q. Nguyen, T. Q. *J. Phys. Chem. C* **2008**, *112*, 7054–7061.
(26) Pu, K. Y.; Liu, B. *Adv. Funct. Mater.* **2009**, *19*, 1371–1378.
(27) He, F.; Feng, F. D.; Wang, S.; Li, Y. L.; Zhu, D. B. *J. Mater. Chem.* **2007**, *17*, 3702–3707.
(28) Lee, K. W.; Povlich, L. K.; Kim, J. S. *Adv. Funct. Mater.* **2007**, *17*, 2580–2587.
(29) Lee, K. W.; Cho, J. C.; DeHeck, J.; Kim, J. S. *Chem. Commun.* **2006**, 1983–1985.
(30) Tu, G. L.; Li, H. B.; Forster, M.; Heiderhoff, R.; Balk, L. J.; Sigel, R.; Scherf, U. *Small* **2007**, *3*, 1001–1006.
(31) (a) Scherf, U.; Gutacker, A.; Koenen, N. *Acc. Chem. Res.* **2008**, *41*, 1086–1097. (b) Gutacker, A.; Adamczyk, S.; Helfer, A.; Garner, L. E.; Evans, R. C.; Fonseca, S. M.; Knaapila, M.; Bazan, G. C.; Burrows, H. D.; Scherf, U. *J. Mater. Chem.* **2010**, *20*, 1423–1430.
(32) (a) Wang, D. L.; Gong, X.; Heeger, P. S.; Rininsland, F.; Bazan, G. C.; Heeger, A. J. *Proc. Natl. Acad. Sci. U.S A.* **2002**, *109*, 49–53. (b) Dwight, S. J.; Gaylord, B. S.; Hong, J. W.; Bazan, G. C. *J. Am. Chem. Soc.* **2004**, *126*, 16850–16859. (c) Tan, C. Y.; Atas, E.; Müller, J. G.; Pinto, M. P.; Kleiman, V. D.; Schanze, K. S. *J. Am. Chem. Soc.* **2004**, *126*, 13685–13694. (d) Müller, J. G.; Atas, E.; Tan, C. Y.; Schanze, K. S.; Kleiman, V. D. *J. Am. Chem. Soc.* **2006**, *128*, 4007–4016. (e) Liao, J. H.; Swager, T. M. *Langmuir* **2007**, *23*, 112–115. (f) Wang, Y. S.; Liu, B. *Chem. Commun.* **2007**, 3553–3555. (g) Chemburu, S.; Ji, E.; Casana, Y.; Wu, Y.; Buranda, T.; Schanze, K. S.; Lopez, G. P.; Whitten, D. G. *J. Phys. Chem. B* **2008**, *112*, 14492–14499. (h) Fang, Z.; Pu, K. Y.; Liu, B. *Macromolecules* **2008**, *41*, 8380–8387. (i) Wang, J.; Liu, B. *Chem. Commun.* **2009**, 2284–2286. (j) Wang, Y. Y.; Liu, B. *Langmuir* **2009**, *25*, 12787–12793. (k) Chen, Y.; Pu, K. Y.; Fan, Q. L.; Qi, X. Y.; Huang, Y. Q.; Lu, X. M.; Huang, W. *J. Polym. Sci., Part A: Polym. Chem.* **2009**, *47*, 5057–5067. (l) Yuan, W. Z.; Zhao, H.; Shen, X. Y.; Mahtab, F.; Lam, J. W. Y.; Sun, J. Z.; Tang, B. Z. *Macromolecules* **2009**, *42*, 9400–9411. (m) Chen, Q.; Cui, Y.; Zhang, T. L.; Cao, J.; Han, B. H. *Biomacromolecules* **2010**, *11*, 13–19.
(33) (a) Fan, C. H.; Plaxco, K. W.; Heeger, A. J. *J. Am. Chem. Soc.* **2002**, *124*, 5642–5643. (b) Kim, I. B.; Dunkhorst, A.; Bunz, U. H. F. *Langmuir* **2005**, *21*, 7985–7989. (c) Tang, Y. L.; He, F.; Yu, M. H.; Feng, F. D.;

An, L. L.; Sun, H.; Wang, S.; Li, Y. L.; Zhu, D. B. *Macromol. Rapid Commun*. **2006**, *27*, 389–392. (d) Xue, C. H.; Donuru, V. R. R.; Liu, H. Y. *Macromolecules* **2006**, *39*, 5747–5752. (e) Miranda, O. R.; You, C. C.; Phillips, R.; Kim, I. B.; Ghosh, P. S.; Bunz, U. H. F.; Rotello, V. M. *J. Am. Chem. Soc*. **2007**, *129*, 9856–9857. (f) Xue, C. H; Luo, F, T.; Liu, H. Y. *Macromolecules* **2007**, *40*, 6863–6870. (g) Phillips, R. L.; Kim, I. B.; Tolbert, L. M.; Bunz, U. H. F. *J. Am. Chem. Soc*. **2008**, *130*, 6952–6954. (h) Tang, Y. L.; Zhou, Z.; Ogawa, K.; Lopez, G. P.; Schanze, K. S.; Whitten, D. G. *Langmuir* **2009**, *25*, 21–25. (i) Shi, J. B.; Cai, L. P.; Pu, K. Y.; Liu, B. *Chem. Asian J*. **2010**, *5*, 301–308.

(34) (a) Gaylord, B. S.; Heeger, A. J.; Bazan, G. C. *J. Am. Chem. Soc*. **2003**, *125*, 896–900. (b) Liu, B.; Gaylord, B. S.; Wang, S.; Bazan, G. C. *J. Am. Chem. Soc*. **2003**, *125*, 6705–6714. (c) Liu, B.; Baudrey, S.; Jaeger, L.; Bazan, G. C. *J. Am. Chem. Soc*. **2004**, *126*, 4076–4077. (d) Zheng, J.; Swager, T. M. *Chem. Commun*. **2004**, 2798–2799. (e) He, F.; Tang, Y. L.; Wang, S.; Li, Y. L.; Zhu, D. B. *J. Am. Chem. Soc*. **2005**, *127*, 12343–12346. (f) Lee, K. W.; Maisel, K.; Rouillard, J. M.; Gulari, E.; Kim, J. S. *Chem. Mater*. **2008**, *20*, 2848–2850. (g) Liu, B.; Bazan, G. C. *J. Am. Chem. Soc*. **2006**, *128*, 1188–1196. (h) Peng, H.; Soeller, C.; Travas-Sejdic, J. *Chem. Commun*. **2006**, 3735–3737. (i) Wang, Y. S.; Liu, B. *Anal. Chem*. **2007**, *79*, 7214–7220. (j) Jiang, G. X.; Susha, A. S.; Lutich, A. A.; Stefani, F. D.; Feldmann, J.; Rogach, A. L. *ACS Nano* **2009**, *3*, 4127–4131. (k) Li, B. L.; Qin, C. J.; Li, T.; Wang, L. X.; Dong, S. *J. Anal. Chem*. **2009**, *81*, 3544–3550. (l) Wigenius, J. A.; Magnusson, K.; Björk, P.; Andersson, O.; Inganäs, O. *Langmuir* **2010**, *26*, 3753–3759. (m) Xia, F.; Zuo, X.; Yang, R.; Xiao, Y.; Kang, D.; Valle-Blisle, A.; Gong, X.; Heeger, A. J.; Plaxco, K. W. *J. Am. Chem. Soc*. **2010**, *132*, 1252–1254.

(35) Ho, H. A.; Boissinot, M.; Bergeron, M. G.; Corbeil, G.; Doré, K.; Boudreau, D.; Leclerc, M. *Angew. Chem., Int. Ed*. **2002**, *41*, 15481551.

(36) Nilsson, K. P. R.; Inganäs, O. *Nat. Mater*. **2003**, *2*, 419–424.

(37) (a) Ho, H. A.; Leclerc, M. *J. Am. Chem. Soc*. **2004**, *126*, 1384–1387. (b) Tang, Y. L.; Feng, F. D.; Yu, M. H.; An, L. L.; He, F.; Wang, S.; Li, Y. L.; Zhu, D. B.; Bazan, G. C. *Adv. Mater*. **2008**, *20*, 703–705. (c) Xia, F.; Zuo, X. L.; Yang, R. Q.; Xiao, Y.; Kang, D.; Vallee-Belisle, A.; Gong, X.; Yuen, J. D.; Hsu, B. B. Y.; Heeger, A. J.; Plaxco, K. W. *Proc. Natl. Acad. Sci. U.S.A*. **2010**, *117*, 10837–10841.

(38) Nilsson, K. P. R.; Rydberg, J.; Baltzer, L.; Inganäs, O. *Proc. Natl. Acad. Sci. U.S.A*. **2003**, *110*, 10170–10174.

(39) (a) Li, C.; Numata, M.; Takeuchi, M.; Shinkai, S. *Angew. Chem., Int. Ed*. **2005**, *44*, 6371–6374. (b) Yao, Z. Y.; Feng, X. L.; Hong, W. J.; Li, C.; Shi, G. Q. *Chem. Commun*. **2009**, 4696–4698. (c) Yao, Z. Y.; Bai, H.; Li, C.; Shi, G. Q. *Chem. Commun*. **2010**, 5094–5096.

(40) Maynor, M. S.; Nelson, T. L.; Sullivan, C. O.; Lavigne, J. J. *Org. Lett*. **2007**, *9*, 3217–3220.

(41) Yao, Z. Y.; Li, C.; Shi, G. Q. *Langmuir* **2008**, *24*, 12829–12835.

(42) Zhan, R. Y.; Fang, Z.; Liu, B. *Anal. Chem*. **2010**, *82*, 1326–1333.

(43) Liu, B.; Bazan, G. C. *J. Am. Chem. Soc*. **2004**, *126*, 1942–1943.

(44) Hong, J. W.; Hemme, W. L.; Keller, G. E.; Rinke, M. T.; Bazan, G. C. *Adv. Mater*. **2006**, *18*, 878–882.

(45) Chi, C. Y.; Mikhailovsky, A.; Bazan, G. C. *J. Am. Chem. Soc*. **2007**, *129*, 11134–11145.

(46) Pu, K. Y.; Liu, B. *Macromolecules* **2008**, *41*, 6636–6640.

(47) Shi, J. B.; Pu, K. Y.; Zhan, R. Y.; Liu, B. *Macromol. Chem. Phys*. **2009**, *210*, 1195–1200.

(48) Yu, D. Y.; Zhang, Y.; Liu, B. *Macromolecules* **2008**, *41*, 4003–4011.

(49) Satrijo, A.; Swager, T. M. *J. Am. Chem. Soc*. **2007**, *129*, 16020–16028.

(50) An, L. L; Tang, Y. L.; Feng, F. D; He, F.; Wang, S. *J. Mater. Chem*. **2007**, *17*, 4147–4152.

(51) An, L. L.; Wang, S.; Zhu., D. B. *Chem. Asian. J*. **2008**, *3*, 1601–1606.

(52) Wang, F. K.; Bazan, G. C. *J. Am. Chem. Soc*. **2006**, *128*, 15786 15792.

(53) (a) Pu, K. Y.; Liu, B. *Adv. Funct. Mater*. **2009**, *19*, 277–284. (b) Pu, K. Y.; Liu, B. *J. Phys. Chem. B* **2010**, *114*, 3077–3084.

(54) Pu, K. Y.; Cai, L. P.; Liu, B. *Macromolecules* **2009**, *42*, 5933–5940.

(55) Pu, K. Y.; Zhan, R. Y.; Liu, B. *Chem. Commun*. **2010**, *46*, 1470–1472.

(56) (a) Moon, J. H.; McDaniel, W.; Maclean, P.; Hancock, L. F. *Angew. Chem., Int. Ed*. **2007**, *46*, 8223–8225. (b) Wu, C.; Bull, B.; Szymanski, C.; Christensen, K.; McNeill, J. *ACS Nano* **2008**, *2*, 2415–2423. (c) Wu, C.; Bull, B.; Christensen, K.; McNeill, J. *Angew. Chem., Int. Ed*. **2009**, *48*, 2741–2745. (d) Li, K.; Pan, J.; Feng, S. S.; Wu, A. W.; Pu, K. Y.; Liu, Y. T.; Liu, B. *Adv. Funct. Mater*. **2009**, *19*, 3535–3542. (e) Howes, P.; Thorogate, R.; Green, M.; Jickells, S.; Daniel, B. *Chem. Commun*. **2009**, 2490–2492. (f) Klingstedt, T.; Nilsson, K. P. R. *Biochim. Biophys. Acta* **2010**, No. DOI:10.1016/j.bbagen.2010.05.003. (g) Kim, S.; Lim, C. K.; Na, J.; Lee, Y. D.; Kim, K.; Choi, K.; Leary, J. F.; Kwon, I. C. *Chem. Commun*. **2010**, *46*, 1617–1619. (h) Nilsson, K. P. R.; Hammarström, P. *Adv. Mater*. **2008**, *20*, 2639–2645. (i) Tuncel, D.; Demir, H. V. *Nanoscale* **2010**, *2*, 484–494. (j) Pu, K. Y.; Li, K.; Liu, B. *Adv. Mater*. **2010**, *22*, 643–646. (k) Pu, K. Y.; Li, K.; Zhang, X. H.; Liu, B. *Adv. Mater*. **2010**, *22*, 4186–4189.

(57) (a) Nilsson, K. P. R.; Hammarström, P.; Ahlgren, F.; Herland, A.; Schnell, E. A.; Lindgren, M.; Westermark, G. T.; Inganäs, O. *ChemBioChem* **2006**, *7*, 1096–1104. (b) Nilsson, K. P. R.; Åslund, A.; Berg, I.; Nyström, S.; Konradsson, P.; Herland, A.; Inganäs, O.; Stabo-Eeg, F.; Lindgren, M.; Westermark, G. T.; Lannfelt, L.; Nilsson, L. N.; Hammarström, P. *ACS Chem. Biol*. **2007**, *2*, 553–560. (c) Sigurdson, C. J.; Nilsson, K. P. R.; Hornemann, S.; Manco, G.; Polymenidou, M.; Schwarz, P.; Leclerc, M.; Hammarström, P.; Wüthrich, K.; Aguzzi, A. *Nat. Methods* **2007**, *4*, 1023–1030.

(58) Kim, I. B.; Shin, H.; Garcia, A. J.; Bunz, U. H. F. *Bioconjugate Chem*. **2007**, *18*, 815–820.

(59) McRae, R. L.; Phillips, R. L.; Kim, I. B.; Bunz, U. H. F.; Fahrni, C. J. *J. Am. Chem. Soc*. **2008**, *130*, 7851–7853.

(60) Björk, P.; Nilsson, K. P. R.; Lenner, L.; Kågedal, B.; Persson, B.; Inganäs, O.; Jonasson *J. Mol. Cell. Probes* **2007**, *21*, 329–337.

(61) Pu, K. Y.; Li, K.; Shi, J. B.; Liu, B. *Chem. Mater*. **2009**, *21*, 3816–3822.

(62) Pu, K. Y.; Li, K.; Liu, B. *Adv. Funct. Mater*. **2010**, *20*, 2770–2777.

(63) Feng, X. L.; Tang, Y. L.; Duan, X. R.; Liu, L. B.; Wang, S. *J. Mater. Chem*. **2010**, *20*, 1312–1316.

(64) O'Regan, B. C.; Grätzel, M. *Nature* **1991**, *353*, 737–740.

(65) O'Regan, B. C.; Durrant, J. *Acc. Chem. Res*. **2009**, *42*, 1799–1808.

(66) Mishra, A.; Fischer, M. K. R.; Bauerle, P. *Angew. Chem., Int. Ed*. **2009**, *48*, 2474–2499.

(67) Mwaura, J. K.; Zhao, X. Y.; Jiang, H.; Schanze, K. S.; Reynolds, J. R. *Chem. Mater*. **2006**, *18*, 6109–6111.

(68) Taranekar, P.; Qiao, Q.; Jiang, H.; Ghiviriga, I.; Schanze, K. S.; Reynolds, J. R. *J. Am. Chem. Soc*. **2007**, *129*, 8958–8959.

(69) Liu, X. Z.; Zhu, R.; Zhang, Y.; Liu, B.; Ramakrishna, S. *Chem. Commun*. **2008**, 3789–3791.

(70) Zhang, W.; Fang, Z.; Su, M.; Saeys, M.; Liu, B. *Macromol. Rapid Commun*. **2009**, *30*, 1533–1537.

(71) (a) Peet, J.; Kim, J. Y.; Coates, N. E.; Ma, W. L.; Moses, D.; Heeger, A. J.; Bazan, G. C. *Nat. Mater*. **2007**, *6*, 497–500. (b) Coakley, K. M.; McGehee, M. D. *Chem. Mater*. **2004**, *16*, 4533–4542. (c) Brabec, C. J.; Sariciftci, N. S.; Hummelen, J. C. *Adv. Funct. Mater*. **2001**, *11*, 15–26. (d) Yu, G; Gao, J.; Hummelen, J. C.; Wudl, F.; Heeger, A. J. *Science* **1995**, *270*, 1789–1791. (e) Sariciftci, N. S.; Smilowitz, L.; Heeger, A. J.; Wudl, F. *Science* **1992**, *258*, 1474–1476.

(72) Luo, J.; Wu, H. B.; He, C.; Li, A. Y.; Yang, W.; Cao, Y. *Appl. Phys. Lett*. **2009**, *95*, 043301.

(73) He, C.; Zhong, C. M.; Wu, H. B.; Yang, R. Q.; Yang, W.; Huang, F.; Bazan, G. C.; Cao, Y. *J. Mater. Chem*. **2010**, *20*, 2617–2622.

(74) (a) Oh, S. H.; Na, S. I.; Jo, J.; Lim, B.; Vak, D.; Kim, D. Y. *Adv. Funct. Mater*. **2010**, *20*, 1977–1983. (b) Na, S. I.; Oh, S. H.; Kim, S. S.; Kim, D. Y. *Org. Electron*. **2009**, *10*, 496–500.

(75) Rider, D. A.; Worfolk, B. J.; Harris, K. D.; Lalany, A.; Shahbazi, K.; Fleischauer, M. D.; Brett, M. J.; Buriak, J. M. *Adv. Funct. Mater*. **2010**, *20*, 2404–2415.

(76) Hoven, C. V.; Yang, R. Q.; Garcia, A.; Crockett, V.; Heeger, A. J.; Bazan, G. C.; Nguyen, T. Q. *Proc. Natl. Acad. Sci. U.S.A*. **2008**, *105*, 12730–12735.

(77) Hoven, C. V.; Peet, J.; Mikhailovsky, A.; Nguyen, T. Q. *Appl. Phys. Lett*. **2009**, *94*, 033301.

(78) Park, J.; Hoven, C. V.; Yang, R. Q.; Cho, N. S.; Wu, H. B.; Nguyen, T. Q.; Bazan, G. C. *J. Mater. Chem*. **2009**, *19*, 211–214.

(79) (a) Wu, H. B.; Huang, F.; Peng, J.; Cao, Y. *Org. Electron*. **2005**, *6*, 118–128. (b) Hou, L. T.; Huang, F.; Zeng, W. J.; Peng, J. B.; Cao, Y. *Appl. Phys*. **2005**, *87*, 153509. (c) Shen, H. L.; Huang, F.; Hou, L. T.; Wu, H. B.; Cao, W.; Yang, W.; Cao, Y. *Synth. Met*. **2005**, *152*, 257–260. (d) Wu, H. B.; Huang, F.; Mo, Y.; Yang, W.; Wang, D.; Peng, J.; Cao, Y. *Adv. Mater*. **2004**, *16*, 1826–1830.

(80) (a) Seo, J. H.; Nguyen, T. Q. *J. Am. Chem. Soc*. **2008**, *130*, 10042–10043. (b) Seo, J. H.; Yang, R. Q.; Brzezinski, J. Z.; Walker, B.; Bazan, G. C.; Nguyen, T. Q. *Adv. Mater*. **2009**, *21*, 1006–1011.

(81) Park, J.; Yang, R. Q.; Hoven, C. V.; Garcia, A.; Fischer, D. A.; Nguyen, T. Q.; Bazan, G. C.; DeLongchamp, D. M. *Adv. Mater*. **2008**, *20*, 2491–2496.

(82) Steuerman, D. W.; Garcia, A.; Dante, M.; Yang, R.; Lofvander, J. P.; Nguyen, T. Q. *Adv. Mater*. **2008**, *20*, 528–534.

(83) Wang, C.; Garcia, A.; Yan, H. P.; Sohn, K. E.; Hexemer, A.; Nguyen, T. Q.; Bazan, G. C.; Kramer, E. J.; Ade, H. *J. Am. Chem. Soc*. **2009**, *131*, 12538–12539.

(84) (a) Shi, W.; Jiang, X.; Zen, W. J.; Huang, F.; Yang, W.; Liu, R. S.; Cao, Y. *Macromol. Chem. Phys*. **2009**, *210*, 150–160. (b) Shi, W.; Wang, L.; Huang, F.; Liu, R. S.; Yang, W.; Cao, Y. *Polym. Int*. **2009**, *58*, 373–379.

(85) Garcia, A.; Brzezinski, J. Z.; Nguyen, T. Q. *J. Phys. Chem. C* **2009**, *113*, 2950–2954.

(86) Seo, J. H.; Gutacker, A.; Walker, B.; Cho, S. N.; Garcia, A.; Yang, R. Q.; Nguyen, T. Q.; Heeger, A. J.; Bazan, G. C. *J. Am. Chem. Soc*. **2009**, *131*, 18220–18221.

(87) (a) Natali, D.; Fumagalli, L.; Sampietro, M. *J. Appl. Phys*. **2007**, *101*, 014501. (b) Scheinert, S.; Paasch, G. *J. Appl. Phys*. **2009**, *105*, 014509. (c) Boudinet, D.; Blevennec, G. L.; Serbutoviez, C.; Verilhac, J.-M.; Yan, H.; Horowitz, G. *J. Appl. Phys*. **2009**, *105*, 084501. (d) Cho, S.; Seo, J. H.; Lee, K.; Heeger, A. J. *Adv. Funct. Mater*. **2009**, *19*, 1459–1464.

(88) (a) Cheng, C. H.; Lonergan, M. C. *J. Am. Chem. Soc*. **2004**, *126*, 10536–10537. (b) Pfeiffer, M.; Leo, K.; Zhou, X.; Huang, J. S.; Hofmann, M.; Werner, A.; Blochwitz-Nimoth, J. *Org. Electron*. **2003**, *4*, 89103.

(89) Robinson, S. G.; Johnston, D. H.; Weber, C. D.; Lonergan, M. C. *Chem. Mater*. **2010**, *22*, 241–246.

(90) Hoven, C. V.; Wang, H. P.; Elbing, M.; Garner, L.; Winkelhaus, D.; Bazan, G. C. *Nat. Mater*. **2010**, *9*, 249–252.